LITHOS 466-467 (2024) 107465

Contents lists available at ScienceDirect

LITHOS

journal homepage: www.elsevier.com/locate/lithos

Mantle-like to low oxygen isotopes in zircon from the mid-Cretaceous high-silica granites reveal unweathered basement recycling along the present coastal area of SE China

Hang Xu, Xiao-Lei Wang *, Yue Guan

State Key Laboratory for Mineral Deposits Research, School of Earth Sciences and Engineering, Frontiers Science Center for Critical Earth Material Cycling, Nanjing University, Nanjing 210023, China

ARTICLE INFO

Keywords:
Zircon
Oxygen isotopes
Low-$\delta^{18}O$ granite
Peralkaline granite
SE China

ABSTRACT

Zircon oxygen isotope compositions can provide potential constraints on the origin of granitic magmas. In this work, we report new data of zircon U—Pb dating, trace elements and Hf—O isotopes for two types of mid-Cretaceous high-silica granites from Zhoushan archipelago in Zhejiang Province, SE China. The in-situ zircon data are carefully screened for radiation damage and post-magmatic alteration. The analyzed magmatic zircon grains indicate that the Zhoushan calc-alkaline granites (ZCAG; 101–92 Ma) have mantle-like $\delta^{18}O$ values of 5.29–5.88 ‰, in contrast to the Zhoushan peralkaline granites (ZPAG; 91–89 Ma) with relatively low $\delta^{18}O$ of 4.42–4.6 ‰. The slight decreases in $\delta^{18}O$ and $\varepsilon_{Hf}(t)$ from zircon center to periphery of both groups suggest that they may have consistent oxygen isotopic compositions in their parental magma sources and have gone through assimilations to hydrothermally altered wall rocks in the shallow crust. The mantle-like $\delta^{18}O$ values in zircon are widespread in the Cretaceous felsic rocks in the present coastal area of SE China, which, in combination Hf isotopes, indicates the possible existence of a buried unweathered Proterozoic basement in the eastern part of the Cathaysia Block. This work highlights the role of deep crustal magma sources, assimilation and post-magmatic radioactive damage on the formation of mantle-like to low $\delta^{18}O$ signals in zircons, and has fundamental implications for understanding the formation of widespread mid-Cretaceous felsic rocks along the present coastal area of SE China.

1. Introduction

Granite is the most widely distributed rock type on the Earth's continental crust, and is also unique among the known terrestrial planets (e.g., Campbell and Taylor, 1983; Rudnick, 1995). Understanding the origin of granite is crucial to studying the formation and evolution of continental crust (e.g., Hawkesworth and Kemp, 2006a; Rudnick, 1995; Wang, 2017), the genesis and exploration of endogenetic metallic deposits (e.g., Linnen and Cuney, 2005; Liu et al., 2020a; Wang, 2017), and the formation of large felsic volcanic provinces (e.g., Bachmann and Bergantz, 2008). Available studies of experimental petrology and geochemical modeling have built a strong relationship between granite formation and the reworking of pre-existing diverse crustal materials, including mantle-derived juvenile crust, (meta)sedimentary rocks, or their mixture. However, the nature of granitic magma sources remains controversial from case to case because of the scarcity of direct links between granites and magma sources in the field and the complexity in interpreting whole-rock geochemistry, which also hinders the understanding of the significance of granite in crustal formation and evolution (e.g., Kemp et al., 2006; Wang et al., 2013).

Oxygen is the most abundant element in the Earth's crust and its isotopic composition can provide potential constraints on the origin of granitic magmas (e.g., Taylor and Sheppard, 1986; Hawkesworth and Kemp, 2006b; Bindeman, 2008). It is generally accepted that magma differentiation has a slightly / limitedly positive effect on the $\delta^{18}O$ value of melts (e.g., Bindeman, 2008; Bindeman et al., 2004; Taylor and Sheppard, 1986; Valley, 2003). In high-silica melts, this positive trend flattens since the chemical compositions of the crystalline phases are as same as the residual melts (Bindeman, 2008; Bindeman et al., 2004). Zircon has been widely used as the premier tracer in terms of O isotopes in felsic magmas (e.g., Valley, 2003) because of the physical and chemical resistance of pristine crystalline zircon and slow oxygen

* Corresponding author.
E-mail address: wxl@nju.edu.cn (X.-L. Wang).

https://doi.org/10.1016/j.lithos.2023.107465
Received 28 November 2023; Received in revised form 3 December 2023; Accepted 12 December 2023
Available online 17 December 2023

diffusion rates (e.g., Cherniak and Watson, 2003; Page et al., 2007; Valley et al., 1994). The mantle is a reservoir with remarkably homogeneous oxygen isotopes and crystalline zircon from mantle-derived melts has a narrow range of $\delta^{18}O = 5.3 \pm 0.6$ ‰ (2SD; Valley et al., 2005). However, with magmatic differentiation from basaltic to rhyolitic in composition, the fractionation factor, $\Delta^{18}O$ (zircon – whole rock), may be as low as −2 ‰ (Valley et al., 1994, 2005). It means that felsic melts evolved from mantle-derived magmas can potentially crystallize zircon with $\delta^{18}O$ of 4 ‰. Therefore, the zircon crystallized from mantle-derived melts and their differentiated products could have $\delta^{18}O$ values of 4–6.3 ‰ (mantle-derived zircon; e.g., Bindeman et al., 2004; Wang et al., 2013; Blum et al., 2016) and thus zircon with $\delta^{18}O$ values below 4 ‰ is generally considered as low-$\delta^{18}O$ zircon. These features imply that O isotopes may provide important clues for the explanations of lithosphere-hydrosphere interaction and granite petrogenesis.

Voluminous felsic granites and rhyolites are developed along the present coastal area of SE China, with ages mainly of Early to Middle Cretaceous. In recent years, more in-situ oxygen isotope data in zircon were published and it is known some cala-alkaline (A/NK > 1; Al_2O_3 (molar)/($Na_2O + K_2O$) (molar)) granites in the area have slightly higher $\delta^{18}O$ values than that of their associated peralkaline granites (A/NK < 1), for example, the cala-alkaline granites of Fuzhou and Shadi ($\delta^{18}O$ of 5–5.8 ‰) and peralkaline granite of Kuiqi ($\delta^{18}O$ of 4.7 ‰) (Chen et al., 2019a). Previous studies mainly focused on the genesis of low-$\delta^{18}O$ signals in individual peralkaline granites and interpreted them as the result of extensional setting, radioactive damage and/or magmatic differentiation (e.g., Fan et al., 2021; Gao et al., 2018; Li et al., 2015). However, Early to Middle Cretaceous cala-alkaline and peralkaline granites in SE China share many similarities, such as high silica and similar mineral compositions. The difference in $\delta^{18}O$ between the two types of rocks thus remains controversial, and it is necessary to reevaluate the oxygen isotopes in high-silica granites and their implications on petrogenesis.

Here, we present a systematic and detailed zircon Hf—O isotopic investigation on the middle Cretaceous calc-alkaline and peralkaline granites in Zhoushan archipelago of northeastern Zhejiang Province, SE China. The peralkaline granitic intrusions are spatially associated with the calc-alkaline granitic intrusions, and they together constitute part of the Cretaceous high-silica I–A type composite granite belt along the coastal area of SE China (Gao et al., 2018; Jiang et al., 2022; Xu et al., 2022; Zhao et al., 2016). We emphasize the role of deep crustal magma sources, assimilation and post-magmatic radioactive damage on the formation of mantle-like to low $\delta^{18}O$ signals in zircons. Magmatic zircon data show that both the Zhoushan calc-alkaline and peralkaline granites have the mantle-like $\delta^{18}O$ characteristic in their parental melts and are originally inherited from the crust sources.

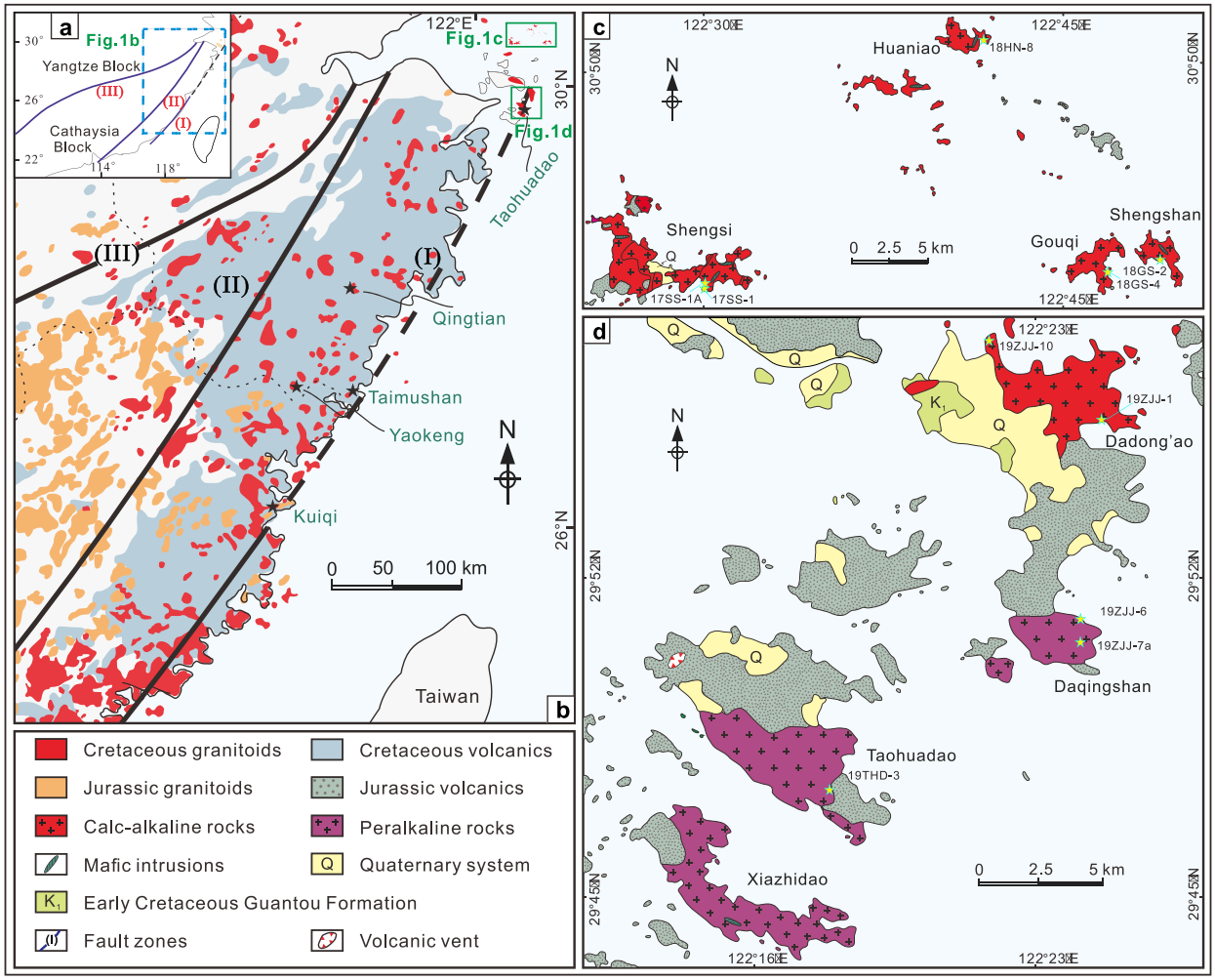

Fig. 1. Simplified geological map. (**a**) The South China Block. (**b**) The distribution of Late Mesozoic igneous rocks in SE China and the location of the studied area (Modified from Zhou et al., 2006). Fault zones: (I)– Changle–Nan'ao fault; (II)– Zhenghe–Dapu fault; (III)– Jiangshan–Shaoxing fault. (**c–d**) Geological maps of the studied areas, northeastern coast of Zhejiang Province (modified after the 1:200, 000 geological maps of Shengsi and Dinghai sheets; BGMRZJ, 1980). The locations of peralkaline rocks are shown.

2. Geological background

The South China Block is commonly thought to have been amalgamated of the Yangtze Block to the northwest and the Cathaysia Block to the southeast by the Jiangnan orogen at 860–820 Ma (Li and Zhao, 2020; Wang et al., 2007, 2014a). After strong crustal reworking by the subsequent tectonic extension, multi-stage Phanerozoic igneous rocks formed in SE China (Liu et al., 2020b; Zhou et al., 2006). Among them, Jurassic felsic rocks are mainly located at inland sites of the Cathaysia Block, while Cretaceous magmatic rocks are generally distributed along the present coastal area of eastern Cathaysia (Fig. 1b; e.g., Liu et al., 2020b), as a response to the westward subduction of paleo-Pacific plate (e.g., Li and Li, 2007). These Cretaceous rocks mainly include rhyolite-dominating bimodal volcanic suites (rhyolite / basalt), I-type granites, mafic dikes and a few peralkaline A-type granite plutons (Fig. 1b). Mantle-derived basic melts are generally thought to have provided heat and sometimes materials for the formation of these felsic rocks (e.g., Zhao et al., 2016; Gao et al., 2018; Chen et al., 2019a, 2019b).

The granite plutons in Zhoushan archipelago of Zhejiang Province are located in the farthest of the Cretaceous granite/volcanic belt of eastern Cathaysia. It is generally considered that their emplacements were controlled by the Changle–Nan'ao fault (Fig. 1b; e.g., Xu et al., 2022; Zhao et al., 2016). The rocks in the archipelago are predominantly composed of mid-Cretaceous high-silica granites and less Jurassic volcanics, as well as a few volcanic and/or volcaniclastic rocks of the Early Cretaceous Guantou Formation and less Late Cretaceous mafic dykes (Fig. 1c–d). The granites intruded into the Jurassic volcanic rocks and/or the Guantou Formation, and were in turn intruded by the mafic dykes. These granites can be geochemically divided into two groups according to available petrography, geochronology and geochemistry: (1) the Zhoushan calc-alkaline granites (ZCAG), i.e., Gouqi, Shengsi, Dadong'ao, Shengshan and Huaniao plutons (this study and Zhao et al., 2016; Xu et al., 2022; Fig. 1c–d); and (2) the Zhoushan peralkaline granites (ZPAG), i.e., Daqingshan and Taohuadao plutons (Zhao et al., 2016; Jiang et al., 2022; Fig. 1d).

3. Samples

Petrology and whole-rock geochemistry of both the ZCAG and ZPAG have been described by Zhao et al. (2016), Jiang et al. (2022) and Xu et al. (2022), and only a brief description is provided below.

The miarolitic cavities (Fig. 2a–b) are common in both ZCAG and ZPAG, suggesting that they both intruded at shallow crustal levels. These rocks can be classified as alkali feldspar granites due to the high amount of K-feldspar (40–55%) relative to plagioclase and besides that, they are composed mainly of quartz (35–50%), biotite (2–5%), and plagioclase (2–8%), with accessory minerals, such as zircon and magnetite. In contrast to the ZCAG, the ZPAG contains arfvedsonite and aegirine (1–2%) and plagioclase is rarely observed. Micrographic intergrowths of quartz and alkali feldspar (granophyric texture; Fig. 2d) are very common, especially in the ZPAG, which is also interpreted as the result of a high-level emplacement (Mushkin et al., 2003). Geochemically, all the rocks are high in silica (SiO_2 = 71.5–78.7 wt%), and the ZPAG even are strongly siliceous (SiO_2 = 76.2–78.7 wt%).

4. Results

Seven ZCAG and three ZPAG samples were collected in this study for analyses of zircon O isotopes, U—Pb dating, trace elements, and Hf isotopes. They are Gouqi (18GS–4), Shengsi (17SS–1 and 17SS–1 A), Dadong'ao (19ZJJ–1 and 19ZJJ–10), Shengshan (18GS–2) and Huaniao (18HN–8) granites for ZCAG, and Daqingshan (19ZJJ–6 and 19ZJJ–7a) and Taohuadao (19THD–3) granites for ZPAG.

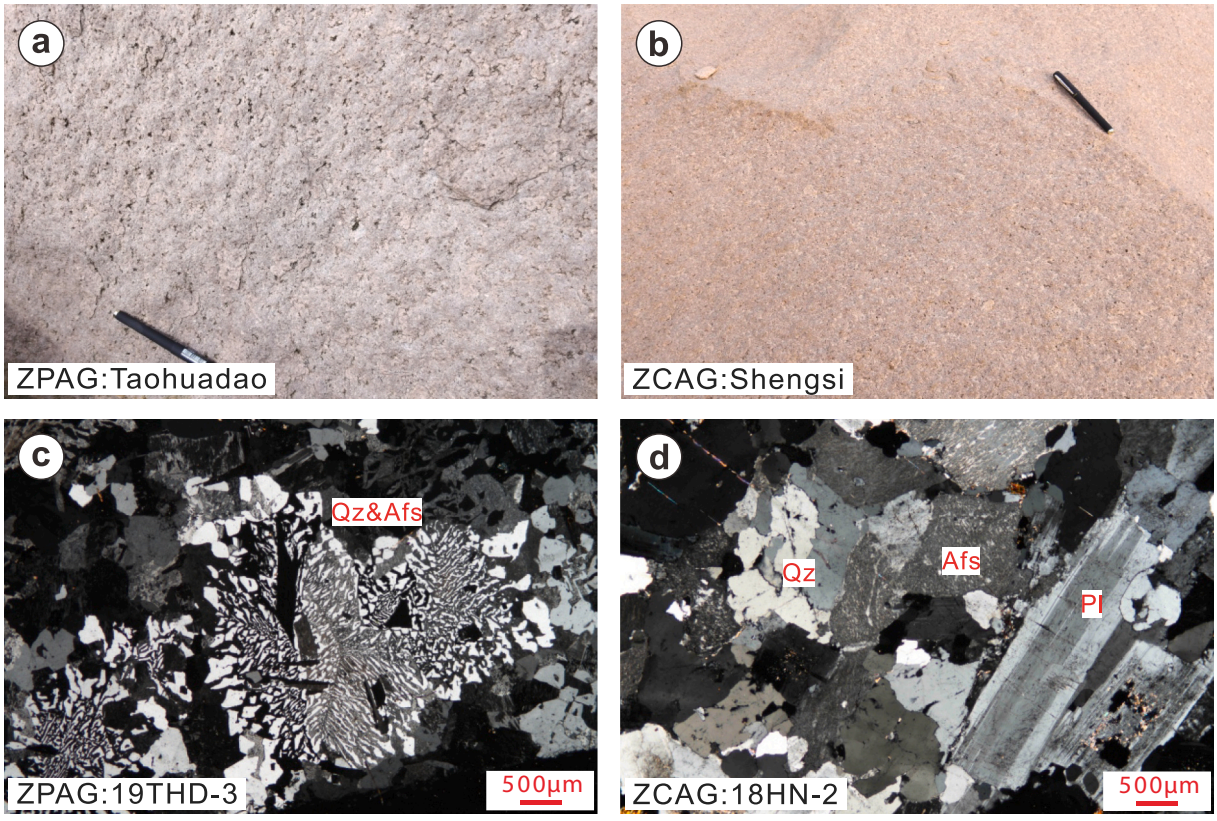

Fig. 2. Macroscopic (**a–b**) and thin section (**c–d**) photographs of representative samples from the Zhoushan granites. (**a**) and (**b**), miarolitic cavities in the ZPAG and the ZCAG, respectively; (**c**) granophyric textures in the ZPAG. Mineral abbreviation: Qz– quartz; Pl– plagioclase; Afs– alkali-feldspar. (**c–d**) under cross-polarized light.

4.1. Zircons morphology, internal texture, trace elements and ages

4.1.1. ZCAG

Zircon grains from sample 18GS–4 from the Gouqi Pluton (ZCAG) are generally colorless to light brown, short prismatic, euhedral to subhedral, 100–250 μm long and have aspect ratios of 1:1 to 2.5:1. In CL images, they show strong CL intensity and typical oscillatory/ sector zoning (Fig. 3a). Most of them have Th/U ratios of 0.9–2.2 and (Th + U) concentrations of 208–1048 ppm (except one high to 2.9 and 1906 ppm, respectively). The chondrite-normalized REE patterns of zircon all show the typical REE patterns of magmatic zircon, with strong enrichments of heavy rare earth elements relative to light REEs, low La concentrations, evident Eu negative anomalies and positive Ce anomalies (Fig. 4). The combination of oscillatory zoning, higher Th/U ratio and REE patterns indicates that those zircon grains are of magmatic origins. Thirteen spot analyses yield a weighted mean of $^{206}Pb/^{238}U$ age of 100.9 ± 1.3 Ma (n = 13, MSWD = 1.09; Fig. 5a).

Zircon grains from samples 17SS–1 A and 17SS–1 of the Shengsi Pluton (ZCAG) have similar morphology, internal texture and trace element characteristics as those in the sample 18GS–4 (Fig. 3a). Among them, zircon grains from 17SS–1 A show Th/U ratios of 0.9–1.8, (Th + U) concentrations of 227–912 ppm and yield a weighted mean age of 98.7 ± 1.4 Ma (n = 12, MSWD = 0.82; Fig. 5b), and those from 17SS–1 have Th/U ratios of 0.3–1.6, (Th + U) concentrations of 418–748 ppm and yield a weighted mean age of 98 ± 1.4 Ma (n = 8, MSWD = 0.63; Fig. 5c).

Zircon grains from samples 19ZJJ–1 and 19ZJJ–10 from the Dadong'ao Pluton (ZCAG) have two types. One is similar to the grains from the Gouqi Pluton (Fig. 3a), with Th/U ratios and (Th + U) concentrations of 1–2.7 and 416–1060 ppm. The other is less in both samples and characterized by (1) euhedral to subhedral crystals, weak CL intensity and typically clear hourglass texture in CL images (Fig. 3b); and (2) high (Th + U) concentrations of 2456–3728 ppm. Their Th/U ratios (1.1–1.3) and REE patterns are indistinguishable from the former type (Fig. 4). Both types are consistent in U—Pb dates for each sample and they yield weighted mean ages of 98.4 ± 1.5 Ma (n = 11, MSWD = 1.2; Fig. 5d) for 19ZJJ–1 and 102.3 ± 4.6 Ma (n = 6, MSWD = 6.6; Fig. 5e) for 19ZJJ–10. The latter mean age has a larger MSWD with spot analyses, and we think the former result is more reliable.

Zircon grains from sample 18GS–2 of the Shengshan Pluton (ZCAG) also show similar characteristics as those from the Gouqi Pluton (Fig. 3a). They have Th/U ratios of 1.1–2.1 and (Th + U) concentrations of 375–1248 ppm. Nine analyses yield a weighted mean age of 96.7 ± 1.4 Ma (n = 9, MSWD = 0.97; Fig. 5f).

Zircon grains from sample 18HN–8 of the Huaniao Pluton (ZCAG) have two types which are similar to the zircon types from the Dadong'ao Pluton respectively. Zircon grains with weak CL intensity are dominant and have high (Th + U) concentrations of 1911–9835 ppm relative to zircon with strong CL intensity and low (Th + U) concentrations of 546–1186 ppm. Both types show similar ranges of Th/U ratios of 0.7–2.2 and 0.8–2.3, respectively. Twelve analyses give a weighted mean age of 92.3 ± 1.3 Ma (n = 12, MSWD = 1.2; Fig. 5g).

4.1.2. ZPAG

Zircon grains from sample 19THD–3 of the Taohuadao Pluton (ZPAG) show similar characteristics to zircons from the Gouqi Pluton (Fig. 3a), but with typically clear hourglass texture in CL images. They have Th/U ratios of 0.8–1.9 and (Th + U) concentrations of 295–1176 ppm. Twelve analyses yield a weighted mean age of 90.5 ± 1.2 Ma (n = 12, MSWD = 0.72; Fig. 5h).

Zircon grains from samples 19ZJJ–6 and 19ZJJ–7a from the Daqingshan Pluton (ZPAG) have three types. The first has similar characteristics to zircon grains from the Taohuadao Pluton (Fig. 3a), with Th/U ratios of 0.9–1.8 and (Th + U) concentrations of 246–1309 ppm. The second has weak CL intensity but is angular and xenomorphic, and most of the internal domains seem disordered in CL images (Fig. 3c). They have Th/U ratios of 1.4–6.5 and high (Th + U) concentrations of 1404–3964 ppm. The third is featured by the spongy-like CL images (Fig. 3d), indicating that they have gone through significant metamictization and recrystallization. Their chemical and isotopic compositions are therefore no longer representative of pristine melts. Only the first type grains were used for U—Pb dating and they give weighted mean ages of 89.3 ± 1.0 Ma (n = 14, MSWD = 1.08; Fig. 5i) for 19ZJJ–6 and 89.3 ± 1.6 Ma (n = 8, MSWD = 1.7; Fig. 5j) for 19ZJJ–7a.

To conclude, the detailed morphological and geochemical characteristics divide the investigated zircon grains from the ZCAG and ZPAG into four types. Type 1 zircon (Fig. 3a) has strong CL intensity and low (Th + U) concentrations (208–1309 ppm; Fig. 4d). Type 2 zircon (Fig. 3b) is featured by weak CL intensity and high (Th + U) concentrations (1911–9835 ppm; Fig. 4d). Both types are used for U—Pb dating and age calculation. Type 3 zircon (Fig. 3c) shows weak CL intensity and high (Th + U) concentrations (1404–3964 ppm; Fig. 4d), but differs from Type 2 zircon by angular and xenomorphic crystal shapes. All three types have similar Th/U ratios (Fig. 4c) and REE patterns (Fig. 4a and b). Type 4 zircon (Fig. 3d) has spongy-like CL images because of the significant metamictization and recrystallization and is not appropriate for in situ isotopic and elemental analysis.

4.2. Zircon Hf and O isotopes

4.2.1. ZCAG

Type 1 zircon from sample 18GS–4 (Gouqi Pluton) has $\varepsilon_{Hf}(t)$ values

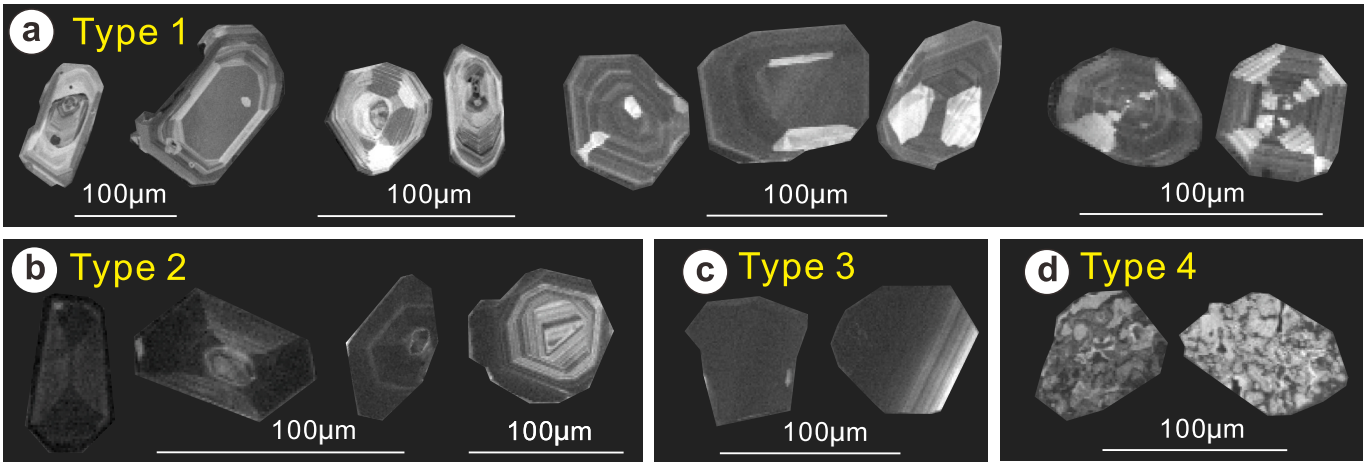

Fig. 3. Representative cathodoluminescence (CL) images of selected zircon grains from the ZCAG and ZPAG.

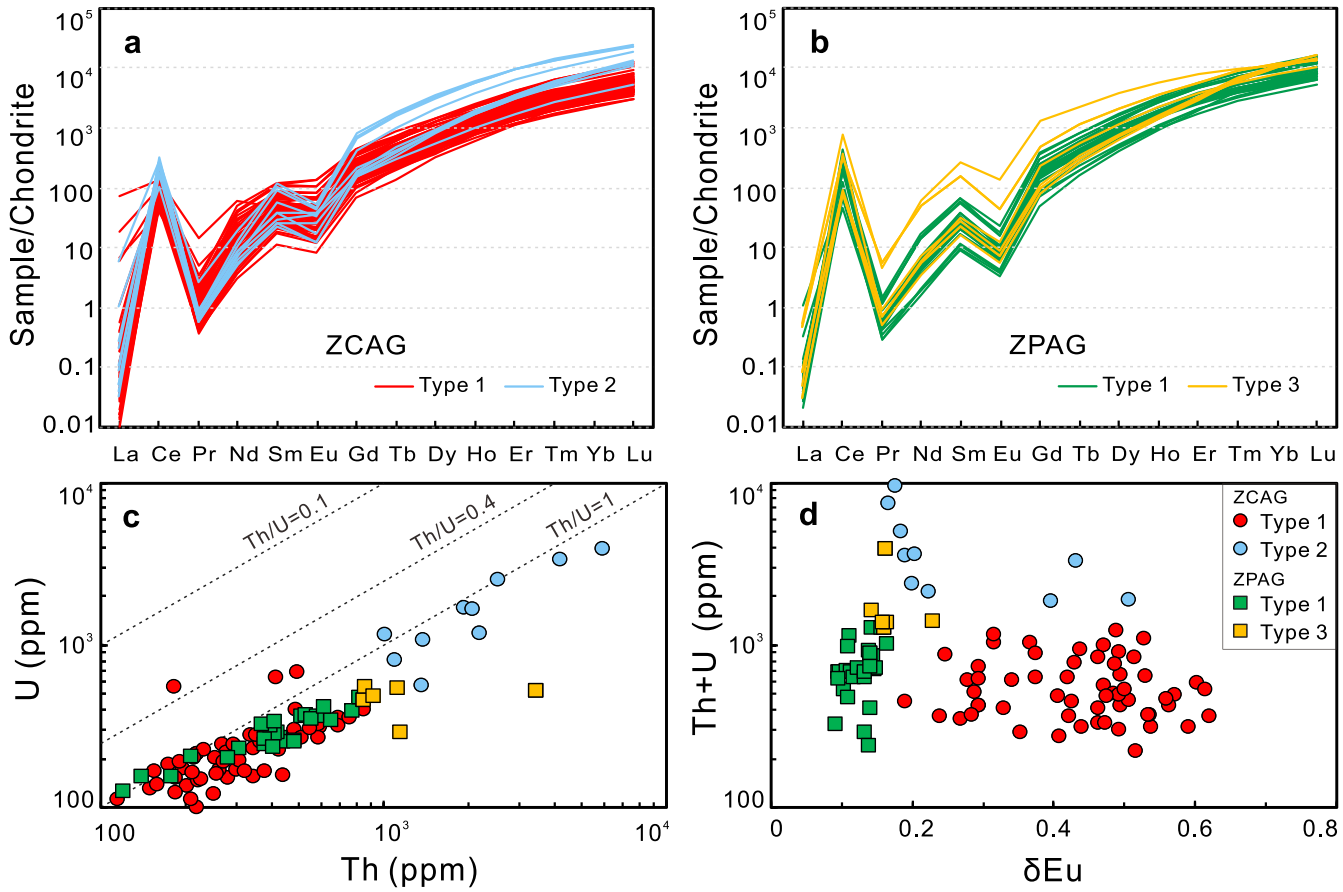

Fig. 4. SIMS zircon trace elements of the studied granites. Chondrite values used for normalization are from McDonough and Sun (1995).

that vary from −5.4 to −2 (Fig. 6a), T_{DM2}(Hf) values of 1500–1300 Ma. Twenty-nine analyses give a weighted mean $\delta^{18}O$ values of 5.72 ± 0.08 ‰ (n = 29, MSWD = 1.1; Fig. 7a).

Type 1 zircon from samples 17SS–1 A and 17SS–1 (Shengsi Pluton) has $\varepsilon_{Hf}(t)$ values of −4.8 to −2 and − 6.9 to −3.2 (Fig. 6b and c), T_{DM2}(Hf) of 1460–1290 Ma and 1600–1370 Ma, respectively. Thirteen analyses of 17SS–1 A have a weighted mean $\delta^{18}O$ values of 5.46 ± 0.14 ‰ (n = 13, MSWD = 0.23; Fig. 7b). Ten analyses of 17SS–1 show a weighted mean $\delta^{18}O$ of 5.32 ± 0.14 ‰ (n = 10, MSWD = 0.07; Fig. 7c).

Type 1 zircon from sample 19ZJJ–1 (Dadong'ao Pluton) shows $\varepsilon_{Hf}(t)$ values ranging from −11.9 to −4.6 (Fig. 6d), T_{DM2}(Hf) values of 1920–1450 Ma, and a weighted mean $\delta^{18}O$ of 5.48 ± 0.13 ‰ (n = 16, MSWD = 0.53; Fig. 7d). Type 1 zircon from sample 19ZJJ–10 has $\varepsilon_{Hf}(t)$ values varying from −12 to −4.3 (Fig. 6e), T_{DM2}(Hf) values of 1900–1435 Ma, and a weighted mean $\delta^{18}O$ of 5.29 ± 0.19 ‰ (n = 11, MSWD = 1.7; Fig. 7e). Type 2 zircons from sample 19ZJJ–10 have $\varepsilon_{Hf}(t)$, T_{DM2}(Hf) and a weighted mean $\delta^{18}O$ of −12 to −8.6 (Fig. 6e), 1930–1670 Ma, and 4.91 ± 0.13 ‰ (n = 11, MSWD = 0.26; Fig. 7e), respectively.

Type 1 zircon from sample 18GS–2 (Shengshan Pluton) has $\varepsilon_{Hf}(t)$ values varying from −5.1 to −1.6 (Fig. 6f), T_{DM2}(Hf) values of 1480–1265 Ma. Twenty-eight analyses yield a weighted mean $\delta^{18}O$ values of 5.88 ± 0.08 ‰ (n = 28, MSWD = 0.73; Fig. 7f).

Type 1 zircon from sample 18HN–8 (Huaniao Pluton) has $\varepsilon_{Hf}(t)$ values of −5.4 – −0.1 (Fig. 6g), T_{DM2}(Hf) values of 1500–1160 Ma, and a weighted mean $\delta^{18}O$ of 5.68 ± 0.16 ‰ (n = 10, MSWD = 0.46; Fig. 7g). Type 2 zircon from 18HN–8 has $\varepsilon_{Hf}(t)$, T_{DM2}(Hf) and a weighted mean $\delta^{18}O$ of −8.3 to +0.2 (Fig. 6g), 1680–1140 Ma, and 5.38 ± 0.13 ‰ (n = 15, MSWD = 0.24; Fig. 6g), respectively.

4.2.2. ZPAG

Type 1 zircon from sample 19THD–3 (Taohuadao Pluton) has $\varepsilon_{Hf}(t)$ values ranging from −8.1 to +0.1 (Fig. 6h), T_{DM2}(Hf) values of 1670–1150 Ma. Fifteen analyses have a weighted mean $\delta^{18}O$ values of 4.60 ± 0.19 ‰ (n = 15, MSWD = 1.6; Fig. 7h).

Type 1 zircon from sample 19ZJJ–6 (Daqingshan Pluton) has $\varepsilon_{Hf}(t)$ values that range from −6 to −2.3 (Fig. 6i), T_{DM2}(Hf) values of 1540–1300 Ma, and a weighted mean $\delta^{18}O$ of 4.55 ± 0.13 ‰ (n = 17, MSWD = 0.76; Fig. 7i). Type 1 zircon from sample 19ZJJ–7a has $\varepsilon_{Hf}(t)$ values varying from −7.3 to −1.5 (Fig. 6j), T_{DM2}(Hf) values of 1615–1250 Ma, and a weighted mean $\delta^{18}O$ of 4.42 ± 0.16 ‰ (n = 12, MSWD = 1.2; Fig. 7j). Type 3 zircon from 19ZJJ–7a has $\varepsilon_{Hf}(t)$, T_{DM2}(Hf) and a weighted mean $\delta^{18}O$ of −10 to −4.1 (Fig. 6j), 1800–1415 Ma, and 3.71 ± 0.14 ‰ (n = 9, MSWD = 0.17; Fig. 7j), respectively.

5. Discussion

5.1. The effect of radiation damage on zircon oxygen isotopes

Since the physical and chemical resistance of pristine crystalline zircon and slow oxygen diffusion rates (e.g., Cherniak and Watson, 2003; Page et al., 2007; Valley et al., 1994), zircon oxygen isotopes are generally regarded as the robust records of magmatic compositions (e.g., Valley, 2003; Wang et al., 2013). However, recent studies in peralkaline granites have highlighted the possible effects of radioactive damage on oxygen isotopes of zircon with high Th and U concentrations. For example, Gao et al. (2018) suggested that the low-$\delta^{18}O$ zircon ($\delta^{18}O$ of 3.08–4.12 ‰) from the Taohuadao peralkaline granites (belong to ZPAG) may have developed through massive recrystallization promoted by the presence of magma-derived fluids, and they proposed that only the zircon domains with $\delta^{18}O$ of 4.81–5.32 ‰ maintain their primary

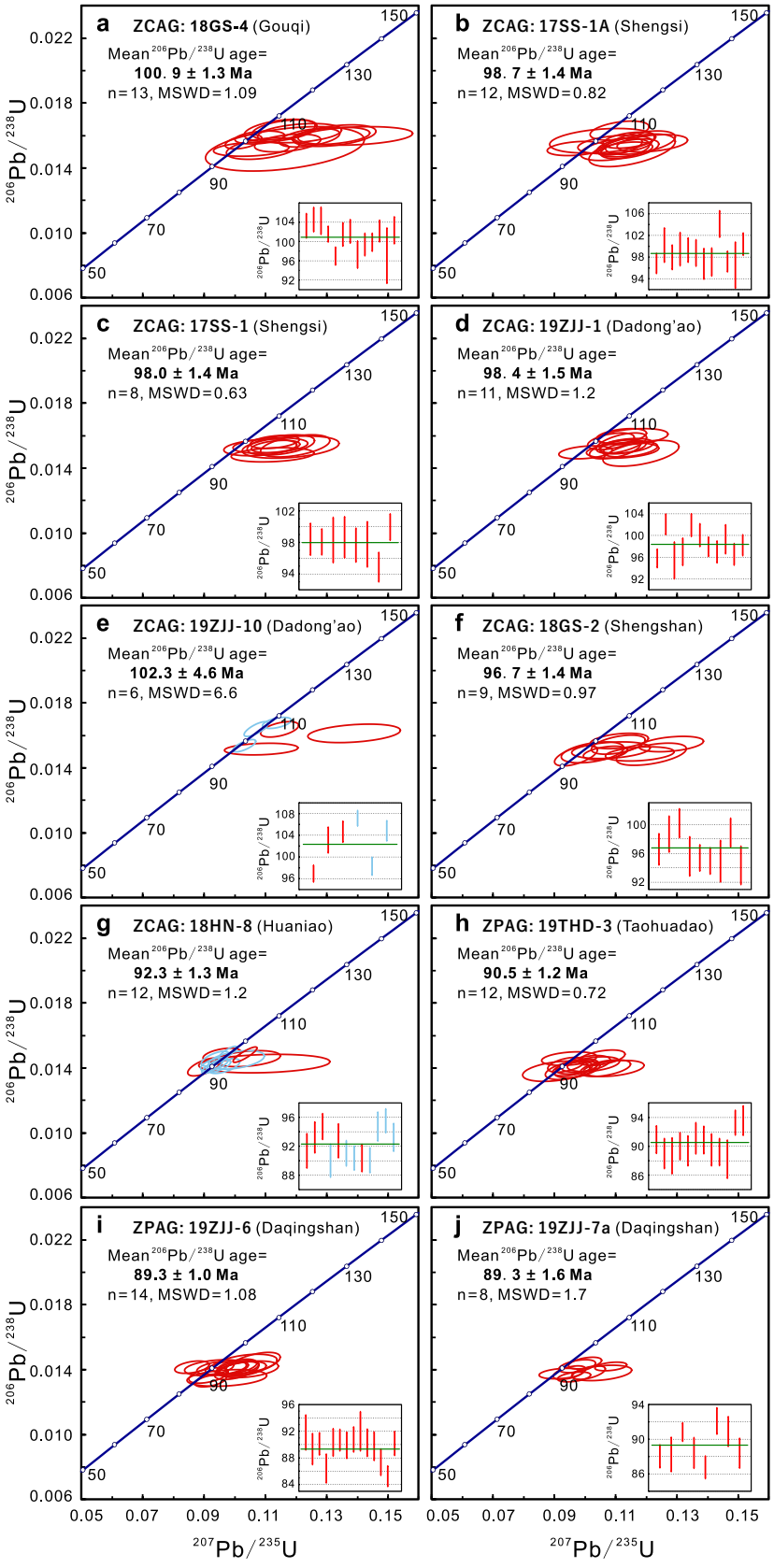

Fig. 5. SIMS zircon U—Pb concordia diagrams of the studied granites. Red analyses are from Type 1 zircons and blue analyses are from Type 2 zircons. (For interpretation of the references to colour in this figure legend, the reader is referred to the web version of this article.)

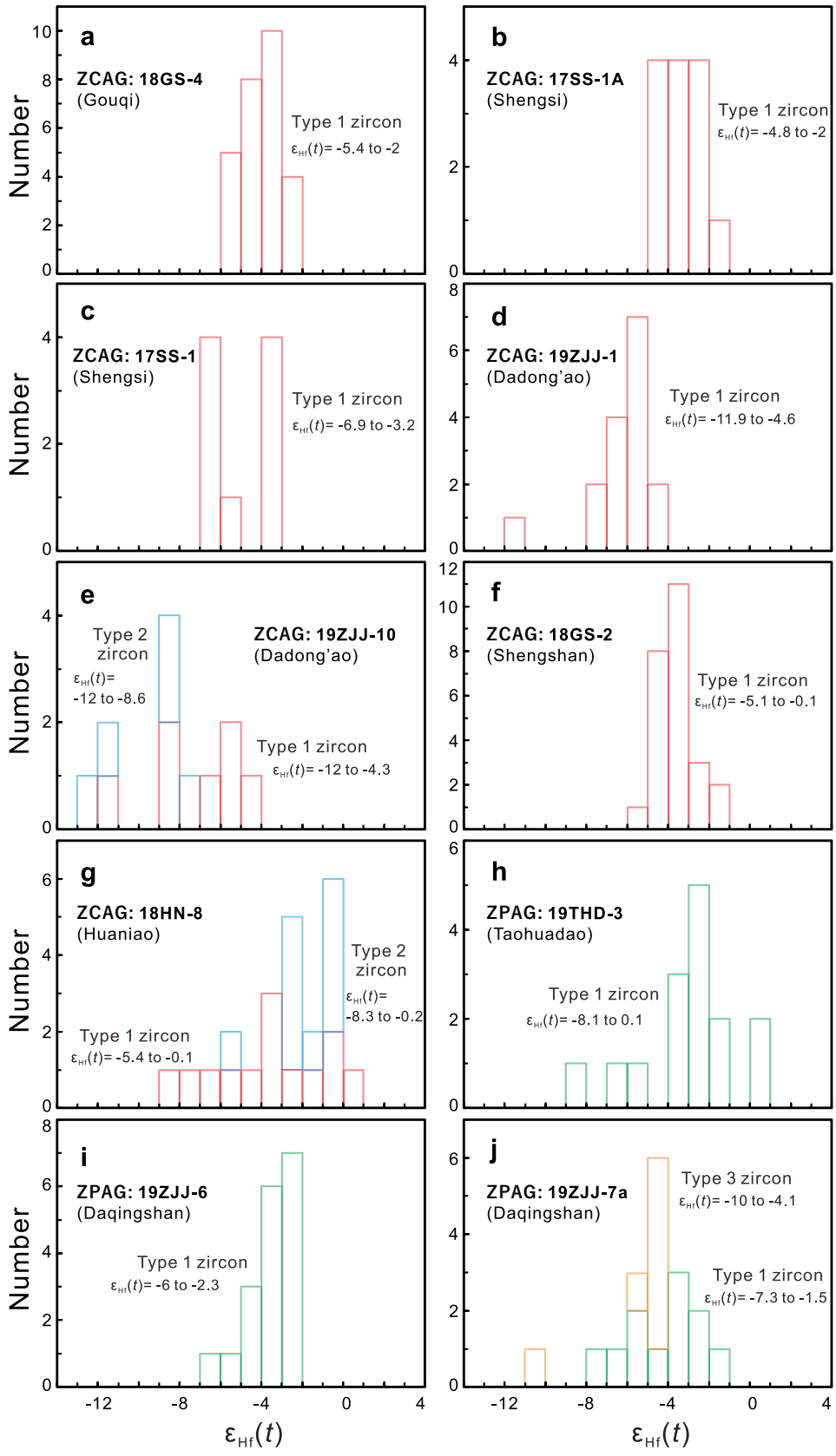

Fig. 6. Histograms of zircon $\varepsilon_{Hf}(t)$ values of the studied granites.

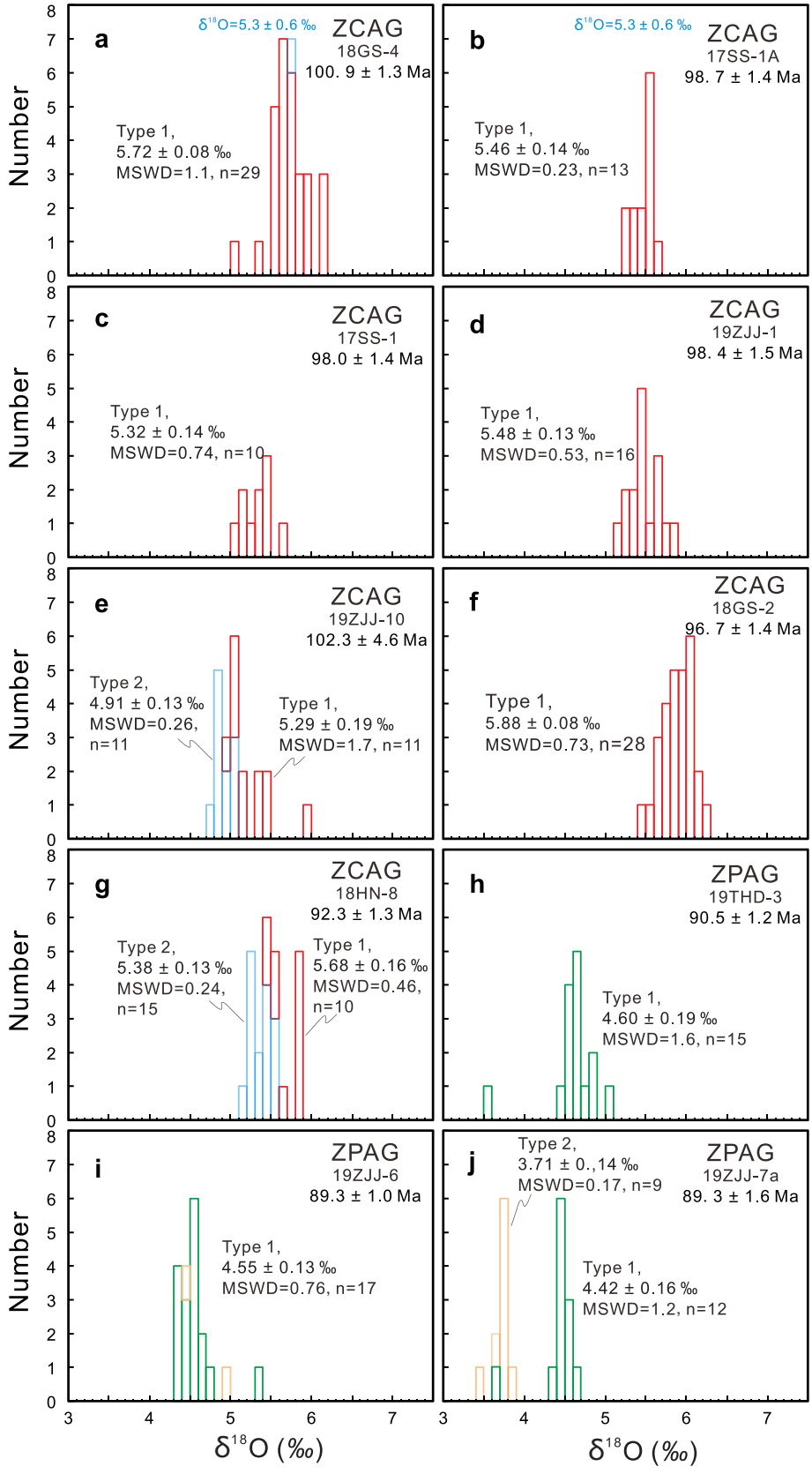

Fig. 7. Histograms of zircon $\delta^{18}O$ values of the ZCAG and the ZPAG.

magmatic characteristics. Fan et al. (2021) suggested that mantle-like to low zircon $\delta^{18}O$ values from the Fengning peralkaline granites in Hebei Province, North China, resulted from the modification to various degrees by meteoric water after the accumulation of radiation damage, and they inferred that only the zircon domains with slightly higher $\delta^{18}O$ than normal mantle could represent their primary magmatic oxygen isotope compositions. Therefore, it is necessary to first evaluate the effects of radiation damage on zircon oxygen isotopes.

Type 1 and Type 2 zircon grains generally show mantle-like $\delta^{18}O$ values, but the $\delta^{18}O$ values of Type 2 are slightly lower than those of Type 1 in the same sample (Fig. 7e and g). Significantly, Type 3 zircon grains from the ZPAG (19ZJJ–7a) have $\delta^{18}O$ values low to 3.71 ‰ (Fig. 7j), which can be classified as low-$\delta^{18}O$ zircons ($\delta^{18}O < 4$ ‰). Trace element analyses indicate that the Th and U concentrations in Type 2 and 3 zircon grains are higher than those in Type 1 (Fig. 4 and Fig. 8), which is also consistent with the strong CL intensity of Type 1 and weak CL intensity of both Type 2 and Type 3. Therefore, although the three types all have steep REE patterns like typical magmatic zircon, the weak CL intensity and high (Th + U) concentrations of both Type 2 and Type 3 zircon indicate that they probably formed in the late-stage granitic melts that are enriched in fluids and incompatible elements, and are therefore at risk of radiation damage accumulation.

Th and U concentrations and internal textures of zircon are effective measures of possible radiation damage. Fan et al. (2021) reported that zircon grains suffered radiation damage generally show a negative correlation between zircon $\delta^{18}O$ values and the U and Th concentrations. However, the expected negative correlations between zircon $\delta^{18}O$ and U, Th or (Th + U) concentrations are not evident in Type 2 or Type 3 zircons (Fig. 8a–c). Nevertheless, all the Type 2 crystals are euhedral to subhedral and show oscillatory zoning and clear hourglass texture in CL images (Fig. 3b), in contrast to the angular and xenomorphic crystals and disordered internal structure of Type 3 zircon. The combination of high (Th + U) concentrations, angular and xenomorphic crystals and disordered internal structure implies that Type 3 zircon grains may have gone through massive recrystallization. This is also supported by Raman spectra results from Gao et al. (2018), in which Type 3 zircon has characteristics of amorphous silica/glass. Therefore, the low-$\delta^{18}O$ values of Type 3 zircon are the result of post-magmatic modification and cannot represent the primary magmatic oxygen isotope compositions. Although Type 2 zircon retains internal structural characteristics of their magmatic origin, it is also challenging for Type 2 zircon $\delta^{18}O$ to represent primary magmatic oxygen isotopic compositions because of their undistinguishable high (Th + U) concentrations with Type 3 zircon grains. On this basis, the oxygen isotopes of Type 1 zircon grains are more representative of the nature of parental magmas.

5.2. *Lower $\delta^{18}O$ signals in peralkaline granites*

As mentioned above, mantle-derived melts can potentially crystallize zircon with $\delta^{18}O$ of 4–6.3 ‰ in high-silica magmas (e.g., Bindeman et al., 2004; Blum et al., 2016; Wang et al., 2013). Type 1 zircon grains from the ZCAG have $\delta^{18}O$ values of 5.29–5.88 ‰, in contrast to the lower $\delta^{18}O$ of 4.42–4.6 ‰ from the ZPAG. Although these values are still within the $\delta^{18}O$ range of mantle-derived zircon, the difference in oxygen isotopic compositions between the two types of rocks is visible, whatever the similarity of zircon $\varepsilon_{Hf}(t)$ values (Fig. 8d) which indicates the similarity of magma sources. Therefore, detailed studies are needed to evaluate the oxygen isotopes.

In-situ oxygen isotope analyses from the center to the periphery of Type 1 zircon reveal the variations of oxygen isotopes during the magmatic evolution. For the same zircon grain from ZCAG, although O isotope analyses for the center and periphery domains (29 pairs) show statistically consistent results within errors, it is noted that the $\delta^{18}O$ values in the center domains are generally higher than those in the periphery domains (23 of 29 pairs; Fig. 9a). Such slight decrease from center to periphery is also evident for the ZPAG zircon grains (7 of 8 pairs; Fig. 9a). The tendency indicates that the general decrease of $\delta^{18}O$ values in ZCAG and ZPAG melts during zircon crystallizing. The possible mechanisms can be categorized as: (1) reduction on magma $\delta^{18}O$ derived by fractional crystallization; (2) infiltration and contamination

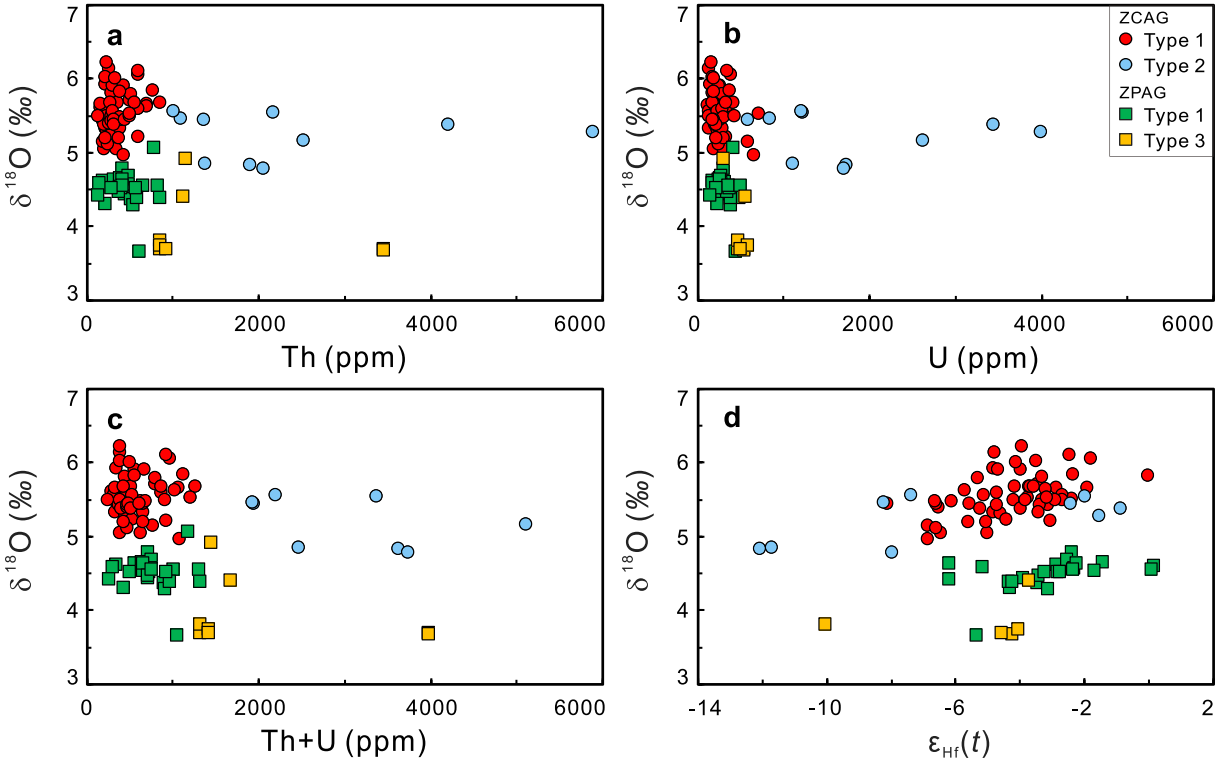

Fig. 8. Diagrams of zircon $\delta^{18}O$ values vs. zircon Th, U and (Th + U) contents and $\varepsilon_{Hf}(t)$ values.

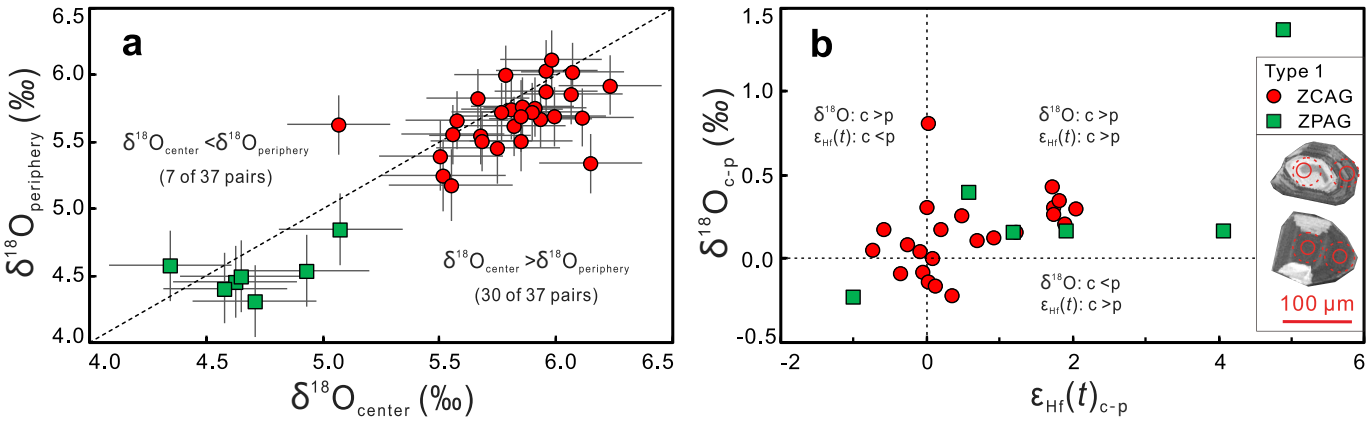

Fig. 9. Zircon $\delta^{18}O$ and $\varepsilon_{Hf}(t)$ values of Type 1 zircons analyzed on center and periphery domains.

of surface water to the magma systems; (3) assimilation of hydrothermally altered wall rocks during magma cooling (e.g., Gao et al., 2018; Hildreth et al., 1984; Taylor, 1977; Taylor and Sheppard, 1986; Valley, 2003).

The reduction of magma $\delta^{18}O$ by fractional crystallization has been used to explain the formation of the lower zircon $\delta^{18}O$ from the Taohuadao peralkaline granites. Gao et al. (2018) suggested that the Taohuadao peralkaline granites (magmatic zircon $\delta^{18}O$ of 4.81–5.23 ‰) are produced by intensive fractionation of reduced and anhydrous basaltic melts and the crystallization of minerals drives a slight depletion on ^{18}O in later crystallized zircons. However, Lee and Morton (2015) proposed that high-silica melts from crystal fractionation of basaltic magmas only account for up to 5% of the original mass of parental magmas. Such a low productivity of high-silica melt directly from basaltic magmas is inconsistent with the absence of outcropped large-scale basalt or accompanied intermediate rocks in Zhoushan archipelago. The negative zircon $\varepsilon_{Hf}(t)$ values and Proterozoic Hf model ages of the ZCAG and ZPAG also preclude a dominant mantle origin but suggest a crustal source instead. Regarding to the decrease of $\delta^{18}O$ from zircon center to the periphery in both the ZCAG and ZPAG, it is inconsistent with that normal magmatic differentiation should shift the $\delta^{18}O$ to higher values and this trend is limited in high-silica melts because of the similar chemical compositions of the crystalline phase and the residual melts (Bindeman et al., 2004). It follows that even considering the unique geochemistry of peralkaline melts, the decrease of $\delta^{18}O$ derived by crystallization differentiation is unlikely to be a good explanation.

The mechanism of infiltration and contamination of surface water to magma system is rarely mentioned to explain the decrease on magma $\delta^{18}O$ values. It is generally accepted that the middle Cretaceous felsic rocks in SE China were emplaced at depths of 7–3 km in an extensional environment (e.g., Chen et al., 2021a; Lowenstern et al., 1997; Xu et al., 2022; Zhao et al., 2016). This formation depth may be within the effective meteoric hydrothermal circulation and/or alteration in the upper crust (e.g., Blum et al., 2016; Ingebritsen and Manning, 2010). However, it is highly challenging to allow massive water to enter the cooling magma (e.g., Hildreth et al., 1984; Taylor, 1977). Oxygen exchanges between the cooling magma and massive surface water require to sustain access and mixing of water with the magma, and significant convection of the magma reservoir to avoid local water saturation (Hildreth et al., 1984). Neither of these is likely to occur in ZCAG and ZPAG because: (1) keeping access and mixing of water and magma requires recurrent explosive activity (Hildreth et al., 1984); (2) magma reservoir of high-silica granites has weak convection (e.g., Bachmann and Bergantz, 2008; Xu et al., 2022); and (3) zircon $\varepsilon_{Hf}(t)$ values also vary from center to periphery (Fig. 9b). Therefore, the decrease of $\delta^{18}O$ during zircon crystallizing is unlikely to be resulted by infiltration and contamination of surface water to the magma systems.

The zircon Hf isotopes corresponding to the oxygen isotope analyses on zircon "center and periphery" provide a breakthrough for the question. For the same zircon grain, although most Hf isotopes from center to periphery show consistent results within errors, it is worth noting that the $\varepsilon_{Hf}(t)$ values of zircon centers are generally higher than those of its peripheries (18 of 23 pairs for the ZCAG and 5 of 6 for the ZPAG; Fig. 9b), suggesting that other components with lower $\delta^{18}O$ and $\varepsilon_{Hf}(t)$ may have entered the cooling magma systems. Rocks with low-$\delta^{18}O$ values are produced by high-temperature hydrothermal alteration near the Earth's surface, and there are no low-$\delta^{18}O$ igneous rocks found in SE China to suggest any low-$\delta^{18}O$ magma source in deep crust (e.g., Yan et al., 2016; Chen et al., 2017, 2019a, 2019b, 2021a, 2021b; Jiang et al., 2018; Gao et al., 2018; Zhang et al., 2018; Fig. 10 and Fig. 11a). Therefore, such small variations in zircon Hf—O isotopes is more likely to occur in shallower magma reservoir rather than inherited from deep magma source. Assimilation with hydrothermally altered wall rocks can well explain the slight decrease of $\delta^{18}O$ and $\varepsilon_{Hf}(t)$ from zircon center to periphery domains. Southeastern China is characterized by extensive and intense magmatic activities during the Cretaceous, which is conducive to high-temperature water-rock reactions near the surface to form low $\delta^{18}O$ rocks as wall rocks of following felsic magmas. Alternatively, the wall rocks are located within the effective meteoric hydrothermal circulation and/or alteration in the upper crust (e.g., Blum et al., 2016; Ingebritsen and Manning, 2010) and thus may contain a small amount of permeated surface water. Assimilation with hydrothermally altered and/or water-bearing wall rocks can decrease the $\delta^{18}O$ and $\varepsilon_{Hf}(t)$ values of magmas together.

Assimilation with hydrothermally altered wall rocks can also explain the slightly lower $\delta^{18}O$ in the ZPAG than that in the ZCAG. Based on the data of Gao et al. (2018) and this study, the zircon $\delta^{18}O$ values from ZPAG vary from 4.42 ‰ to 5.23 ‰ and its initial melts have similar $\delta^{18}O$ to that of the ZCAG melts (this study and Gao et al., 2018). We suggest that assimilation reduces the oxygen isotopes of ZPAG to 4.42 ‰. Previous studies and our observations indicate that both ZPAG and ZCAG have shallow emplacement depths, and ZPAG was emplaced at a shallower crustal level than that of ZCAG (e.g., Xu et al., 2022; Zhao et al., 2016). This is consistent with the viewpoint that the formation of ZPAG is the response to further lithospheric extension (e.g., Zhao et al., 2016). Due to the influence of permeability / porosity of the crust, the shallower wall rocks are more capable of oxygen exchange during hydrothermally altered and thus generate lower oxygen isotopes of magmas. On this basis, we suggest that the ZPAG initial melts could have originally the indistinguishable mantle-like$\delta^{18}O$ values as the ZCAG melts.

5.3. *Source nature of mantle-like to low-$\delta^{18}O$ felsic rocks in SE China*

Both the ZCAG and the ZPAG, as discussed above, are from the crust materials with mantle-like and indistinguishable $\delta^{18}O$, and formed in an extensional environment due to the subduction rollback of the paleo-

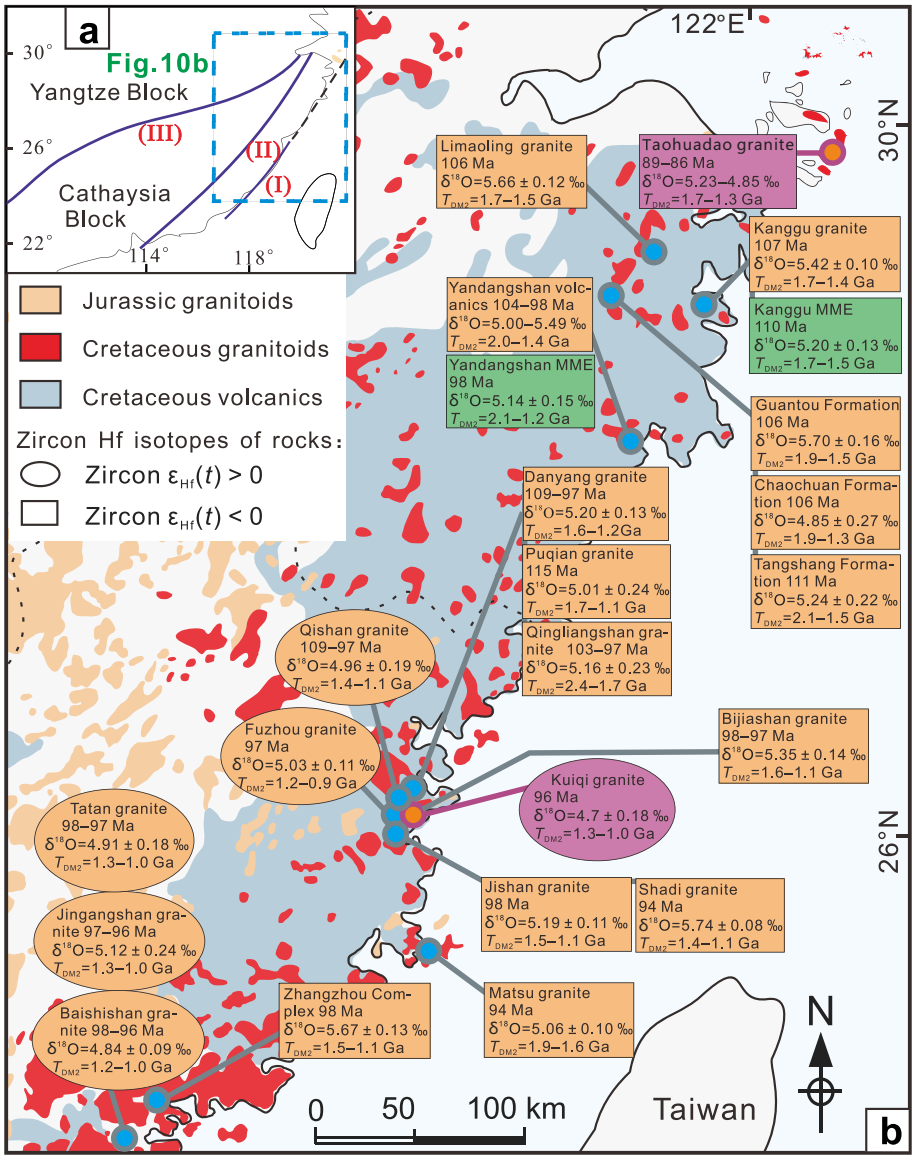

Fig. 10. Zircon ages, T_{DM2}(Hf) and $\delta^{18}O$ values of Cretaceous volcanic–plutonic rocks. $\delta^{18}O$ values refer to the ranges of weight means (2SD). *Purple*: peralkaline granites; *orange*: calc-alkaline felsic rocks; *green*: mafic microgranular enclave (MME). Data from Yan et al. (2016), Chen et al. (2017, 2019a, 2019b, 2021a, 2021b), Jiang et al. (2018), Zhang et al. (2018) and Gao et al. (2018). (For interpretation of the references to colour in this figure legend, the reader is referred to the web version of this article.)

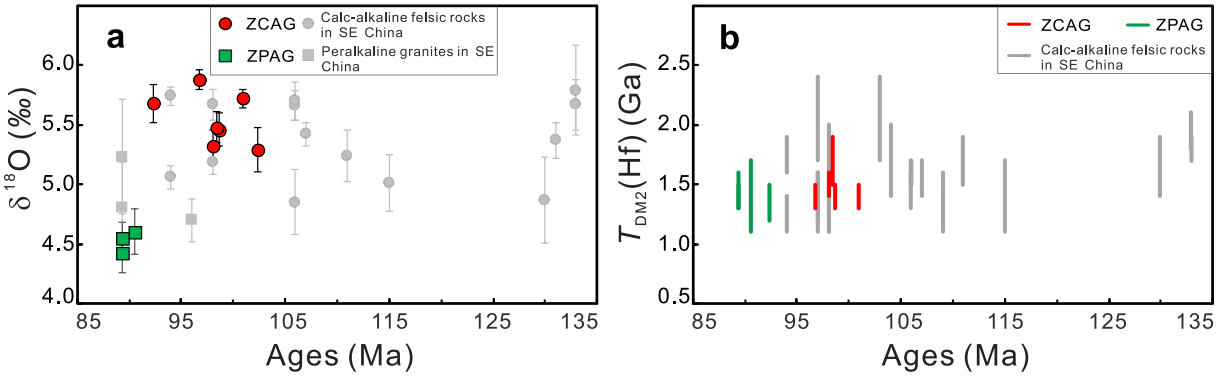

Fig. 11. (**a**) Weighted mean zircon $\varepsilon_{Hf}(t)$ values of the ZCAG and ZPAG. (**b**) Weighted mean zircon $\delta^{18}O$ values vs. zircon U—Pb ages. Error bars refer to 2SD. All the rocks here have enriched zircon Hf isotopes ($\varepsilon_{Hf}(t) < 0$). Data from this study, Yan et al. (2016), Zhao et al., 2016, Chen et al. (2017, 2019a, 2019b, 2021a, 2021b), Jiang et al. (2018), Zhang et al. (2018), Gao et al. (2018) and Xu et al. (2022).

Pacific plate (e.g., Liu et al., 2020b; He and Xu, 2012). Such oxygen isotopic compositions and background are consistent with those of other Cretaceous (particularly mid-Cretaceous) volcanic–plutonic rocks along the present coastal area of SE China ($\delta^{18}O$ of 4.7–5.67 ‰; e.g., Yan et al., 2016; Chen et al., 2017, 2019a, 2019b, 2021a, 2021b; Jiang et al., 2018; Gao et al., 2018; Zhang et al., 2018; Fig. 10 and Fig. 11a). However, the neighboring Jurassic granites located at the inland sites of the Cathaysia Block generally have higher $\delta^{18}O$ values (6.6–9.9 ‰), which indicates that a larger proportion of supracrustal crust has been incorporated into the magma sources (e.g., Chen et al., 2017; Guo et al., 2012; Liu et al., 2020c; Wang et al., 2014b; Wang et al., 2022; Zhang et al., 2015, 2017; Zhang et al., 2018; Zhao et al., 2017). The origin of widespread felsic magmatism with mantle-like $\delta^{18}O$ values and Proterozoic Hf model ages needs to be extensively studied with two possible mechanisms.

The first possible mechanism is "two-stage modifications" on oxygen isotopes in magma sources. In the first stage, like Jurassic granites, sedimentary materials were added into the magma sources to elevate $\delta^{18}O$ values; and in the second stage, the magma sources suffered high-temperature hydrothermal alteration to decrease their $\delta^{18}O$ to mantle-like values. However, this is highly unlikely because any change in $\delta^{18}O$ associated with meteoric hydrothermal systems is notoriously heterogeneous and spatially complex, which is contrary to the consistent zircon $\delta^{18}O$ values with mantle-like and relative narrow variation of 5.29–5.88 ‰ of the Cretaceous felsic rocks (Fig. 10 and Fig. 11a).

The second mechanism seeks the existence of voluminous unweathered juvenile crust or its reworking magmatic products since they are expected to retain the mantle oxygen isotope signatures and could be further melted to form felsic rocks with mantle-like $\delta^{18}O$ values. In this regard, the enriched Hf isotope compositions ($\varepsilon_{Hf}(t) < 0$) in zircon (Fig. 7a; this study and Yan et al., 2016; Chen et al., 2017, 2019a, 2019b, 2021a, 2021b; Zhao et al., 2016; Jiang et al., 2018; Gao et al., 2018; Zhang et al., 2018; Xu et al., 2022) could be used to trace crust–mantle differentiation ages of sources. Overall normal distribution of Hf isotope model ages precludes a crust–mantle mixed source but supports an origin of Proterozoic crust (Fig. 11b). The slightly variable $\varepsilon_{Hf}(t)$ and T_{DM2}(Hf) values could be resulted from disequilibrium melting (Tang et al., 2014; Wang et al., 2021) or inherited from the crustal source since continental arc magmas could have elevated Hf model ages but keep mantle-like oxygen isotopes. Anyhow, the oxygen isotope inheritance implies the existence of widespread unweathered Proterozoic juvenile crust or its intracrustal reworking magmatic rocks with mantle-like $\delta^{18}O$ in the present coastal area of SE China. The reworking of such unweathered basements could take place at different stages and locations in Cretaceous so that the observed felsic rocks all show consistent mantle-like $\delta^{18}O$ values over time and space (Fig. 10 and Fig. 11a).

The mechanism of "unweathered juvenile crust" can also explain the difference in oxygen isotopes for the Cretaceous and Jurassic felsic rocks. Xu et al. (2007) proposed that the Cathaysia Block in SE China can be subdivided into the eastern and western parts by the boundary of Zhenghe–Dapu fault (Fig. 1a and b), based on the U—Pb dating and Hf isotopes from detrital zircons. Eastern and western Cathaysia have distinct patterns of crustal evolution and may represent two micro-continents that were separated before Cambrian time. It is noted that the main body of Cretaceous felsic rocks with mantle-like $\delta^{18}O$ is located in eastern Cathaysia (e.g., Liu et al., 2020b), in contrast to massive Jurassic felsic rocks with higher $\delta^{18}O$ in the western Cathaysia (e.g., Zhou et al., 2006; Guo et al., 2012; Wang et al., 2014b; Zhang et al., 2015, 2017; Yan et al., 2016; Chen et al., 2017, 2019a, 2019b, 2021a, 2021b; Zhao et al., 2017; Jiang et al., 2018; Zhang et al., 2018; Liu et al., 2020b; Wang et al., 2022). Therefore, the difference of O isotopes also implies that the eastern and western Cathaysia have different crustal basements. Considering the common incorporation of crustal materials in the mantle-derived magmas in continental arcs, the Hf model ages may be elevated by several hundreds of million years than the crystallizing ages of the source rocks, which is very significant for the Neoproterozoic granitic rocks in the Jiangnan orogen (Wang et al., 2014a). The Mesoproterozoic (Fig. 11b) model ages may indicate the existence of Neoproterozoic unweathered juvenile crust terrane in the present coastal area of SE China, which may be originally formed by continental arc magmatism.

5.4. Tectonic implications of the mantle-like to low-$\delta^{18}O$ rocks in SE China

The formation of regional mantle-like $\delta^{18}O$ felsic rocks has profound tectonic implications. The widespread Late Mesozoic felsic rocks in SE China can be investigated in terms of oxygen isotopes. According to available data, the oxygen isotopes of the Late Mesozoic felsic rocks show obvious variations in space and time, i.e., the Jurassic rocks located in the inland area generally have higher $\delta^{18}O$ values (6.6–9.9 ‰; e.g., Guo et al., 2012; Wang et al., 2014b; Zhang et al., 2015, 2017; Chen et al., 2017; Zhao et al., 2017; Zhang et al., 2018; Liu et al., 2020c; Wang et al., 2022), in contrast to the Cretaceous (particularly mid-Cretaceous) volcanic–plutonic rocks along the present coastal area of SE China that have mantle-like $\delta^{18}O$ for their magma source (this study and Yan et al., 2016; Chen et al., 2017, 2019a, 2019b, 2021a, 2021b; Jiang et al., 2018; Gao et al., 2018; Zhang et al., 2018; Fig. 10). The difference in oxygen isotopes of those magmatic rocks may result from the difference of their magma sources. For Cretaceous felsic rocks in the eastern Cathaysia, the oxygen isotope compositions of the rocks with depleted Hf isotopes ($\varepsilon_{Hf}(t) > 0$) in zircon are still more likely to be inherited from the juvenile crust source, such as Zaoshan and Fuzhou granites (e.g., Chen et al., 2014, 2019a), Tatan and Baishishan granites (Chen et al., 2021b). However, voluminous felsic rocks are characterized by enriched Hf isotopes ($\varepsilon_{Hf}(t) < 0$) in zircon and point to the Proterozoic unweathered (juvenile) crustal sources. We suggest that both the calc-alkaline and peralkaline rocks in the eastern Cathaysia have magma sources with mantle-like $\delta^{18}O$ values.

Here, we propose a simplified petrogenetic model for the formation of zircon oxygen isotope differences in the calc-alkaline and peralkaline granites from Zhoushan archipelago of northeastern Zhejiang Province, SE China. During the middle Cretaceous, a rapid high-angle of subducting Paleo-Pacific plate led to the retreat of the trench toward the ocean and consequently formed the back-arc extensional environment. Underplating of mantle-derived magma led to partial melting of preexisting unweathered Neoproterozoic basement or its reworking magmatic products, to form calc-alkaline and peralkaline felsic melts in turn (Fig. 12a). Oxygen isotopic characteristics were inherited in those melts and then the melts ascended and emplaced in the shallow crust. In this process, assimilation to hydrothermally altered and/or water-bearing wall rocks results in a slight decrease in zircon O and Hf isotopes from zircon center to periphery (Fig. 12b and c). In particular, further extension of the crust facilitated the shallower emplacement of the ZPAG melts, helping them decrease oxygen isotopes more quickly to lower than those of the ZCAG (Fig. 12b and c). Nevertheless, the effect of assimilation on oxygen isotopes is slight, so the $\delta^{18}O$ values of those rocks are within the range of mantle-derived zircon (4–6.3 ‰). As for the zircon grains crystallized in the late magma stage, they are enriched in incompatible elements and therefore at risk of potential post-magmatic radioactive damage and modification on oxygen isotopes (Fig. 12b and c). This petrogenetic process is not restricted to Zhoushan mantle-like $\delta^{18}O$ calc-alkaline granites and lower $\delta^{18}O$ peralkaline granites, and can be applied to other similar Cretaceous felsic igneous suites in SE China and other places worldwide.

6. Conclusions

This study presents new dataset of zircon U—Pb dating, trace elements and in situ Hf—O isotopes for the calc-alkaline rocks (ZCAG; 101–92 Ma) and peralkaline rocks (ZPAG; 91–89 Ma) from the Zhoushan archipelago in Zhejiang Province, SE China. Low zircon $\delta^{18}O$ signals in both ZCAG and ZPAG may be caused by post-magmatic

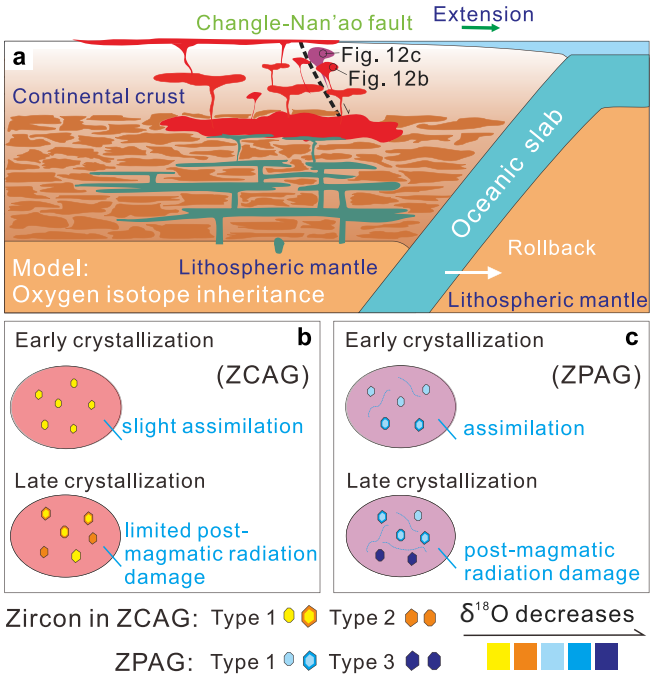

Fig. 12. A schematic illustration shows the genetic model for the formations of oxygen isotope signals in calc-alkaline granites and peralkaline granites during the Cretaceous, SE China. Colour code for $\delta^{18}O$ in the bottom only applies to panels **b** and **c**.

radioactive damage. Screened data show that the magmatic zircon grains have mantle-like $\delta^{18}O$ values of 5.29 ‰ ~ 5.88 ‰ for ZCAG and lower $\delta^{18}O$ values of 4.42 ‰ ~ 4.6 ‰ for ZPAG. The overall decreases of $\delta^{18}O$ and $\varepsilon_{Hf}(t)$ values from zircon center to periphery suggest that the two types of felsic magmas may have consistent oxygen isotopes in their magma sources and have gone through different extents of assimilation with hydrothermally altered wall rocks in shallow crust to result in such $\delta^{18}O$ difference. We suggest the source materials of both could have mantle-like $\delta^{18}O$ values and speculate the existence of a widespread unweathered Neoproterozoic juvenile crust in the present coastal area of SE China. This juvenile terrane may represent the buried main part of the eastern Cathaysia Block and has significant tectonic implications for understanding the Neoproterozoic continent assembly and Mesozoic orogenesis and subduction. We suggest that the model is applied to widespread Cretaceous felsic rocks with mantle-like to low $\delta^{18}O$ and enriched Hf isotopes in zircon, SE China.

Declaration of Competing Interest

The authors declare that they have no known competing financial interests or personal relationships that could have appeared to influence the work reported in this paper.

Data availability

All data used in this study is included within the Supplementary files and corresponding citations.

Acknowledgments

We appreciate Prof. Jian-Sheng Qiu (deceased on 7th July 2020) for his great help for the manuscript. This work was substantially supported by the National Natural Science Foundation of China (Grant Nos. 42025202, 92162322, 41872052), the State Key R&D Project of the Ministry of Science and Technology of China (2022YFF0800402), and the Fundamental Research Funds for the Central Universities (Grant 0206-14380166). The manuscript benefits from constructive comments of two anonymous reviewers and editor Prof. Di-Cheng Zhu.

Appendix A. Analytical methods

All analyses, including zircon O isotopes, U—Pb dating and trace elements, and Hf isotope analyses, were conducted at the State Key Laboratory for Mineral Deposits Research, Nanjing University. Prior to analysis, transmitted and reflected light photomicrographs and cathodoluminescence (CL) images were taken to characterize zircon internal structures. Methods of Hf isotope analyses are in Supplementary files.

A.1. Oxygen isotopes

In situ zircon oxygen isotope analyses for seven ZCAG and three ZPAG samples were undertaken using a CAMECA IMS–1300 HR^3 ion microprobe in the multi-collection mode. A primary $^{133}Cs^+$ ion beam (2.8–3 nA current and 20 keV total impact energy) was focused on the sample surface, with a beam diameter of ~20 μm. A 5 μm × 5 μm raster was used in this study, and a normal-incidence electron gun was used for charge compensation. An NMR field sensor was applied to stabilize the magnetic field. The signals of ^{16}O and ^{18}O were collected simultaneously using two Faraday cups at positions L'2 and H'2 with resistor circuits of 10^{10} Ω and 10^{11} Ω, respectively. The mass resolving power (MRP, M/ΔM), measured at 50% peak height, was set at ~2500 to minimize isobaric interferences. The total analytical time was about 5 min per pit: 100 s pre-sputtering to remove the Au coating, ~ 60 s automatic centering of the secondary ions in the field aperture, and a total of 80 s integration of secondary ions (twenty cycles × 4 s). The counting rate of ^{16}O was approximately 2.9 × 10^9–3.2 × 10^9 cps. Measured $^{18}O/^{16}O$ values were normalized to the Vienna Standard Mean Ocean Water compositions (VSMOW, $^{18}O/^{16}O$ = 0.0020052; Baertschi, 1976). The well characterized zircon standards 91500 ($\delta^{18}O$ = 9.9 ± 0.3 ‰; Wiedenbeck et al., 2004) and TEMORA 2 ($\delta^{18}O$ = 8.20 ± 0.13 ‰; Black et al., 2004) were also analyzed. TEMORA 2 zircon standard was used to correct the instrumental mass fractionation factor (IMF) and 91500 zircon standard was analyzed as unknown samples to ascertain the veracity of the IMF. Forty-four analyses on TEMORA 2 yielded a mean $\delta^{18}O$ = 8.22 ± 0.07 ‰ (2SD, n = 44, MSWD = 0.24), indicating the homogeneity of TEMORA 2 on a split scale or different splits. Twenty-three analyses on 91500 yielded a mean $\delta^{18}O$ = 10.16 ± 0.09 ‰ (2σ, n = 23, MSWD = 0.29), which is consistent within errors with the reported value. Oxygen isotope analyses are shown in Supplementary files with standard deviations of 0.22 ‰ or 0.27 ‰, standard errors (2SE) of 0.10–0.27 ‰ (average of 0.16 ‰).

A.2. SIMS Zircon U—Pb geochronology and trace elements

After oxygen-isotope analyses, sample mount was re-polished and coated. Zircon U—Pb dating and trace elements were generally conducted on the same spots used for O isotope analyses using the same CAMECA IMS–1300 HR^3 ion microprobe. A primary O^{2-} ion beam (6 nA current and 13 keV total impact energy) was focused on the sample surface. A beam diameter was set of ~20 μm and the MRP was ~7000 (50% peak height). Zircon standards 91500 (1062.4 ± 0.4 Ma; Wiedenbeck et al., 1995) and TEMORA 2 (418.3 ± 1.3 Ma; Black et al., 2004) were also analyzed for U—Pb age determinations. Trace element concentrations for zircon were standardized against standard 91500 and the intensities were normalized to $^{28}Si_2^{16}O_2^+$. Detailed analyzing procedures can be referred to Liu et al. (2020c). Repeated measurements of the standards yielded weighted means of $^{206}Pb/^{238}U$ ages of 1065.9 ± 7.1 Ma (2σ, n = 29, MSWD = 0.95) for 91500 and 418.8 ± 4.2 Ma (2σ, n = 33, MSWD = 1.6) for TEMORA 2, which are consistent with the recommended values. Zircon U—Pb dating and trace element results are shown in Supplementary files.

A.3. Zircon Hf isotopes

In situ zircon Hf isotope analyses were conducted on the same spots used for O isotope analyses but with a larger beam diameter of ~44 μm. Hf isotopic compositions were determined using a GeoLas 193 nm ArF_3 laser ablation system attached to a Neptune Plus MC–ICP–MS. Zircons were ablated with a repetition rate of 10 Hz and a pulse energy density of 10.5 J/cm^2. Zircon standards Mud Tank ($^{176}Hf/^{177}Hf = 0.282507 \pm 6$; Woodhead and Hergt, 2005) and 91500 ($^{176}Hf/^{177}Hf = 0.282306 \pm 8$; Wiedenbeck et al., 1995) were analyzed for quality control. Repeated measurements of the standards yielded weighted means of $^{176}Hf/^{177}Hf$ of 0.282506 ± 0.000007 (n = 34, MSWD = 1.14) for Mud Tank and 0.282304 ± 0.000009 (n = 34, MSWD = 0.4) for 91500, which are consistent with the recommended values. The $^{176}Hf/^{177}Hf$ ratios of chondrite (0.282772; Blichert-Toft and Albarède, 1997) and depleted mantle (0.28325; Nowell et al., 1998), $^{176}Lu/^{177}Hf$ ratios of chondrite (0.0332; Blichert-Toft and Albarède, 1997), depleted mantle (0.0384; Griffin et al., 2002) and average continental crust (0.015; Griffin et al., 2002), ^{176}Lu decay constant (1.867 × 10^{-11}/year; Söderlund et al., 2004) and mean zircon U—Pb ages of each granite were used to calculate $\varepsilon_{Hf}(t)$, T_{DM1}(Hf) and T_{DM2}(Hf) values. Results are shown in Supplementary files.

References

Bachmann, O., Bergantz, G.W., 2008. Rhyolites and their Source Mushes across Tectonic Settings. J. Petrol. 49 (12), 2277–2285.

Baertschi, P., 1976. Absolute ^{18}O content of standard mean ocean water. Earth Planet. Sci. Lett. 31, 341–344.

BGMRZJ (Bureau of Geology and Mineral Resources of Zhejiang Province), 1980. Report of Regional Geological Survey: Shengsi, Yuyao, Dinghai. Geological Publishing House, Beijing (in Chinese with English abstract), Ningbo and Shenjiamen breadths.

Bindeman, I.N., 2008. Oxygen isotopes in mantle and crustal magmas as revealed by single crystal analyses. Rev. Mineral. Geochem. 69, 445–478.

Bindeman, I.N., Ponomareva, V.V., Bailey, J.C., Valley, J.W., 2004. Volcanic arc of Kamchatka: a province with high-$\delta^{18}O$ magma sources and large-scale $^{18}O/^{16}O$ depletion of the upper crust. Geochim. Cosmochim. Acta 68, 841–865.

Black, L.P., Kamo, S.L., Allen, C.M., Davis, D.W., Aleinikoff, J.N., Valley, J.W., Mundil, R., Campbell, I.H., Korsch, R.J., Williams, I.S., Foudoulis, C., 2004. Improved $^{206}Pb/^{238}U$ microprobe geochronology by the monitoring of a trace-element-related matrix effect; SHRIMP, ID–TIMS, ELA–ICP–MS and oxygen isotope documentation for a series of zircon standards. Chem. Geol. 205, 115–140.

Blichert-Toft, J., Albarède, F., 1997. The Lu-Hf isotope geochemistry of chondrites and the evolution of the mantle-crust system. Earth Planet. Sci. Lett. 148, 243–258.

Blum, T.B., Kitajima, K., Nakashima, D., Strickland, A., Spicuzza, M.J., Valley, J.W., 2016. Oxygen isotope evolution of the Lake Owyhee volcanic field, Oregon, and implications for the low-$\delta^{18}O$ magmatism of the Snake River Plain–Yellowstone hotspot and other low-$\delta^{18}O$ large igneous provinces. Contrib. Mineral. Petrol. 171, 92.

Campbell, I.H., Taylor, S.R., 1983. No water, no granites - no oceans, no continents. Geophys. Res. Lett. 10 (11), 1061–1064.

Chen, J.Y., Yang, J.H., Zhang, J.H., Sun, J.F., 2014. Geochemical transition shown by cretaceous granitoids in southeastern China: Implications for continental crustal reworking and growth. Lithos 196–197, 115–130.

Chen, J.Y., Yang, J.H., Ji, W.Q., 2017. Agesand petrogenesis of Jurassic and cretaceous intrusive rocks in the Matsu Islands: implications for lower crust modification beneath southeastern China. J. Asian Earth Sci. 150, 14–24.

Chen, J.Y., Yang, J.H., Zhang, J.H., 2019a. Origin of cretaceous aluminous and peralkaline A-type granitoids in northeastern Fujian, coastal region of southeastern China. Lithos 340–341, 223–238.

Chen, J.Y., Yang, J.H., Zhang, J.H., 2019b. Multiple sources of cretaceous granitoids in northeastern Fujian, coastal area of southeastern China. J. Asian Earth Sci. 182, 103939.

Chen, J.Y., Yang, J.H., Zhang, J.H., Sun, J.F., Zhu, Y.S., Hartung, E., 2021a. Generation of cretaceous high-silica granite by complementary crystal accumulation and silicic melt extraction in the coastal region of southeastern China. GSA Bull. 134, B35745.

Chen, J.Y., Yang, J.H., Zhang, J.H., Zhu, Y.S., 2021b. Construction of a highly silicic upper crust in southeastern China: Insights from the cretaceous intermediate-to-felsic rocks in eastern Zhejiang. Lithos 402–403, 106012.

Cherniak, D.J., Watson, E.B., 2003. Diffusion in Zircon. Rev. Mineral. Geochem. 53, 113–143.

Fan, W., Jiang, N., Zhai, M., Hu, J., 2021. Origin of the Low $\delta^{18}O$ Signals in Zircons from the early cretaceous A-Type Granites in Eastern China: evidence from the Kulongshan Pluton. J. Earth Sci. 32 (6), 1415–1427.

Gao, Y.Y., Griffin, W.L., Chu, M.F., O'Reilly, S.Y., Pearson, N.J., Li, Q.L., Liu, Y., Tang, G. Q., Li, X.H., 2018. Constraints from zircon Hf-O-Li isotopic compositions on the genesis of slightly low-$\delta^{18}O$ alkaline granites in the Taohuadao area, Zhejiang Province, SE China. J. Asian Earth Sci. 167, 197–208.

Griffin, W.L., Wang, X., Jackson, S.E., Pearson, S.E., O'Reilly, S.Y., Xu, X.S., Zhou, X.M., 2002. Zircon chemistry and magma genesis, SE China: in situ analysis of Hf isotopes, Tonglu and Pingtan igneous complexes. Lithos 61, 237–269.

Guo, C., Chen, Y., Zeng, Z., Lou, F., 2012. Petrogenesis of the Xihuashan granites in southeastern China: Constraints from geochemistry and in-situ analyses of zircon U \Pb\Hf\O isotopes. Lithos 148, 209–227.

Hawkesworth, C.J., Kemp, A.I.S., 2006a. Evolution of the continental crust. Nature 443 (7113), 811–817.

Hawkesworth, C.J., Kemp, A.I.S., 2006b. Using hafnium and oxygen isotopes in zircons to unravel the record of crustal evolution. Chem. Geol. 226, 144–162.

He, Z.Y., Xu, X.S., 2012. Petrogenesis of the late Yanshanian mantle-derived intrusions in southeastern China: Response to the geodynamics of paleo-Pacific plate subduction. Chem. Geol. 328, 208–221.

Hildreth, W., Christiansen, R.L., Oneil, J.R., 1984. Catastrophic isotopic modification of rhyolitic magma at times of caldera subsidence, Yellowstone plateau volcanic field. J. Geophys. Res. 89, 8339–8369.

Ingebritsen, S.E., Manning, C.E., 2010. Permeability of the continental crust: dynamic variations inferred from seismicity and metamorphism. Geofluids 10, 193–205.

Jiang, X.Y., Ling, M.X., Wu, K., Zhang, Z.K., Sun, W.D., Sui, Q.L., Xia, X.P., 2018. Insights into the origin of coexisting A_1- and A_2-type granites: Implications from zircon Hf-O isotopes of the Huayuangong intrusion in the lower Yangtze River Belt, eastern China. Lithos 318–319, 230–243.

Jiang, D.S., Erdmann, S., Deng, G.X., Guo, H.H., Wu, F., Xu, X.S., Xu, H., Zhao, Z.F., Huang, F., 2022. Barium isotope evidence for the generation of peralkaline granites from a fluid-metasomatized crustal source. Chem. Geol. 614, 121197.

Kemp, A.I.S., Hawkesworth, C.J., Paterson, B.A., Kinny, P.D., 2006. Episodic growth of the Gondwana supercontinent from hafnium and oxygen isotopes in zircon. Nature 439 (7076), 580–583.

Lee, C.A., Morton, D.M., 2015. High silica granites: Terminal porosity and crystal settling in shallow magma chambers. Earth Planet. Sci. Lett. 409, 23–31.

Li, Z.X., Li, X.H., 2007. Formation of the 1300-km-wide intracontinental orogen and postorogenic magmatic province in Mesozoic South China: a flat-slab subduction model. Geology 35, 179–182.

Li, Q.W., Zhao, J.H., 2020. Amalgamation between the Yangtze and Cathaysia blocks in South China: evidence from the ophiolite geochemistry. Precambrian Res. 350, 105893.

Li, Y., Ma, C.Q., Xing, G.F., Zhou, H.W., Zhang, H., Brouwer, F.M., 2015. Origin of a cretaceous low-^{18}O granitoid complex in the active continental margin of SE China. Lithos 216–217, 136–147.

Linnen, R.L., Cuney, M., 2005. Granite-related rare-element deposits and experimental constraints on Ta-Nb-W-Sn-Zr-Hf mineralization. In: Linnen, R.L., Samson, I.M. (Eds.), Rare-Element Geochemistry and Mineral Deposits: Geological Association of Canada, GAC Short Course Notes, vol. 17, pp. 45–67.

Liu, C., Wang, R.C., Wu, F.Y., Xie, L., Liu, X.C., Li, X.K., Yang, L., Li, X.J., 2020a. Spodumene pegmatites from the Pusila pluton in the higher Himalaya, South Tibet: Lithium mineralization in a highly fractionated leucogranite batholith. Lithos 358–359, 105421.

Liu, J.X., Wang, S., Wang, X.L., Du, D.H., Xing, G.F., Fu, J.M., Chen, X., Sun, Z.M., 2020b. Refining the spatio-temporal distributions of Mesozoic granitoids and volcanic rocks in SE China. J. Asian Earth Sci. 201, 104503.

Liu, X., Wang, Q., Ma, L., Wyman, D.A., Zhao, Z.H., Yang, J.H., Zi, F., Tang, G.J., Dan, W., Zhou, J.S., 2020c. Petrogenesis of late Jurassic Pb–Zn mineralized high $\delta^{18}O$ granodiorites in the western Nanling Range, South China. J. Asian Earth Sci. 192, 104236.

Lowenstern, J.B., Clynne, M.A., Bullen, T.D., 1997. Comagmatic A-type granophyre and rhyolite from the Alid volcanic center, Eritrea, northeast Africa. J. Petrol. 38 (12), 1707–1721.

McDonough, W.F., Sun, S.S., 1995. The composition of the Earth. Chem. Geol. 120 (3), 223–253.

Mushkin, A., Navon, O., Halicz, L., Hartmann, G., Stein, M., 2003. The petrogenesis of A-type magmas from the Amram Massif, southern Israel. J. Petrol. 44 (5), 815–832.

Nowell, G.M., Kempton, P.D., Noble, S.R., Fitton, J.G., Saunders, A.D., Mahoney, J.J., Taylor, R.N., 1998. High precision Hf isotope measurements of MORB and OIB by thermal ionization mass spectrometry: insights into the depleted mantle. Chem. Geol. 149, 211–233.

Page, F.Z., Ushikubo, T., Kita, N.Y., Riciputi, L.R., Valley, J.W., 2007. High-precision oxygen isotope analysis of picogram samples reveals 2 μm gradients and slow diffusion in zircon. Am. Mineral. 92, 1772–1775.

Rudnick, R.L., 1995. Making continental crust. Nature 378 (6557), 571–578.

Söderlund, U., Patchett, P.J., Vervoort, J.D., Isachsen, C.E., 2004. The ^{176} Lu decay constant determined by Lu-Hf and U-Pb isotope systematics of Precambrian mafic intrusions. Earth Planet. Sci. Lett. 219, 311–324.

Tang, M., Wang, X.L., Shu, X.J., Wang, D., Yang, T., Gopon, P., 2014. Hafnium isotopic heterogeneity in zircons from granitic rocks: Geochemical evaluation and modeling of "zircon effect" in crustal anatexis. Earth Planet. Sci. Lett. 389, 188–199.

Taylor, H.P., 1977. Water/rock interactions and the origin of H_2O in granitic batholiths. J. Geol. Soc. Lond. 133, 509–558.

Taylor, H.P., Sheppard, S.M.F., 1986. Igneous Rocks: I. Processes of Isotopic Fractionation and Isotope Systematics. Rev. Mineral. Geochem. 16, 227–269.

Valley, J.A., 2003. Oxygen isotopes in zircon. In: Hanchar, J.M., Hoskin, P.W.O. (Eds.), Zircon, Reviews in Mineralogy and Geochemistry, Vol, vol. 53. Mineralogical Society of America, Washington, DC, pp. 1–40.

Valley, J.W., Chiarenzelli, J.R., McLelland, J.M., 1994. Oxygen isotope geochemistry of zircon. Earth Planet. Sci. Lett. 126, 187–206.

Valley, J.W., Lackey, J.S., Cavosie, A.J., Clechenko, C.C., Spicuzza, M.J., Basei, M.A.S., Bindeman, I.N., Ferreira, V.P., Sial, A.N., King, E.M., Peck, W.H., Sinha, A.K., Wei, C.

S., 2005. 4.4 billion years of crustal maturation: oxygen isotopes in magmatic zircon. Contrib. Mineral. Petrol. 150, 561–580.
Wang, X.L., 2017. Some new research progresses and main scientific problems of granitic rocks. Acta Petrol. Sin. 33 (5), 1445–1458 (in Chinese with English abstract).
Wang, X.L., Zhou, J.C., Griffin, W.L., Wang, R.C., Qiu, J.S., O'Reilly, S.Y., Xu, X.S., Liu, X. M., Zhang, G.L., 2007. Detrital zircon geochronology of Precambrian basement sequences in the Jiangnan orogen: dating the assembly of the Yangtze and Cathaysia blocks. Precambrian Res. 159, 117–131.
Wang, X.L., Zhou, J.C., Wan, Y.S., Kitajima, K., Wang, D., Bonamici, C., Qiu, J.S., Sun, T., 2013. Magmatic evolution and crustal recycling for Neoproterozoic strongly peraluminous granitoids from southern China: Hf and O isotopes in zircon. Earth Planet. Sci. Lett. 366, 71–82.
Wang, X.L., Zhou, J.C., Griffin, W.L., Zhao, G.C., Yu, J.H., Qiu, J.S., Zhang, Y.J., Xing, G. F., 2014a. Geochemical zonation across a Neoproterozoic orogenic belt: Isotopic evidence from granitoids and metasedimentary rocks of the Jiangnan orogen, China. Precambrian Res. 242, 154–171.
Wang, X.L., Coble, M.A., Valley, J.W., Shu, X.J., Kitajima, K., Spicuzza, M.J., Sun, T., 2014b. Influence of radiation damage on late Jurassic zircons from southern China: evidence from in situ measurements of oxygen isotopes, laser Raman, U-Pb ages, and trace elements. Chem. Geol. 389, 122–136.
Wang, X.L., Liu, J.X., Lü, Q.T., Wang, S., Wang, D., Chen, X., 2021. Evolution of deep crustal hot zones constrained by the diversity of late Mesozoic magmatic rocks in SE China. Ore Geol. Rev. 134, 104143.
Wang, D., Wang, X.L., Cai, Y., Li, J.Y., Du, D.H., Shu, L.S., 2022. Exploring the Sn–W metallogenic potential of late Jurassic Ganfang-Guyangzhai granite suite, South China: Zircon and apatite geochemistry. Ore Geol. Rev. 144, 104863.
Wiedenbeck, M., Alle, P., Corfu, F., Griffin, W.L., Meier, M., Oberli, F., von Quadt, A., Roddick, J.C., Spiegel, W., 1995. Three natural zircon standards for U–Th–Pb, Lu–Hf, trace element and REE analyses. Geostand. Newslett. 19, 1–23.
Wiedenbeck, M., Hanchar, J.M., Peck, W.H., Sylvester, P., Valley, J., Whitehouse, M., Kronz, A., Morishita, Y., Nasdala, L., Fiebig, J., Franchi, I., Girard, J.P., Greenwood, R.C., Hinton, R., Kita, N., Mason, P.R.D., Norman, M., Ogasawara, M., Piccoli, P.M., Rhede, D., Satoh, H., Schulz-Dobrick, B., Skår, O., Spicuzza, M., Terada, K., Tindle, A., Togashi, S., Vennemann, T., Xie, Q., Zheng, Y.F., 2004. Further Characterisation of the 91500 Zircon Crystal. Geostand. Geoanal. Res. 28, 9–39.
Woodhead, J.D., Hergt, J.M., 2005. A preliminary appraisal of seven natural zircon reference materials for in situ Hf isotope determination. Geostand. Geoanal. Res. 29, 183–195.
Xu, X.S., O'Reilly, S.Y., Griffin, W.L., Pearson, N.J., He, Z.Y., 2007. The crust of Cathaysia: age, assembly and reworking of two terranes. Precambrian Res. 158, 51–78.
Xu, H., Qiu, J.S., Wang, X.L., Hong, Y.F., Wang, R.Q., Li, Y.F., 2022. Slow crystal settling controls the diversity of high-silica granites of the late cretaceous Shengsi Pluton at northeastern tip of Southeast China. J. Asian Earth Sci. 223, 104986.
Yan, L.L., He, Z.Y., Jahn, B., Zhao, Z.D., 2016. Formation of the Yandangshan volcanic–plutonic complex (SE China) by melt extraction and crystal accumulation. Lithos 266–267, 287–308.
Zhang, Y., Yang, J.H., Sun, J.F., Zhang, J.H., Chen, J.Y., Li, X.H., 2015. Petrogenesis of Jurassic fractionated I-type granites in Southeast China: Constraints from whole-rock geochemical and zircon U–Pb and Hf–O isotopes. J. Asian Earth Sci. 11, 268–283.
Zhang, Y., Yang, J.H., Chen, J.Y., Wang, H., Xiang, Y.X., 2017. Petrogenesis of Jurassic tungsten-bearing granites in the Nanling Range, South China: Evidence from whole-rock geochemistry and zircon U–Pb and Hf–O isotopes. Lithos 278–281, 166–180.
Zhang, J.H., Yang, J.H., Chen, J.Y., Wu, F.Y., Wilde, S.A., 2018. Genesis of late early cretaceous high-silica rhyolites in eastern Zhejiang Province, Southeast China: a crystal mush origin with mantle input. Lithos 296–299, 482–495.
Zhao, J.L., Qiu, J.S., Liu, L., Wang, R.Q., 2016. The Late Cretaceous I- and A-type granite association of southeast China: Implications for the origin and evolution of post-collisional extensional magmatism. Lithos 240–243, 16–33.
Zhao, P., Yuan, S., Mao, J., Santosh, M., Zhang, D., 2017. Zircon U–Pb and Hf–O isotopes trace the architecture of polymetallic deposits: A case study of the Jurassic ore-forming porphyries in the Qin–Hang metallogenic belt, China. Lithos 292–293, 132–145.
Zhou, X.M., Sun, T., Shen, W.Z., Shu, L.S., Niu, Y.L., 2006. Petrogenesis of Mesozoic granitoids and volcanic rocks in South China: a response to tectonic evolution. Episodes 29 (1), 26–33.